

Title: Photochemistry beyond the red-limit in chlorophyll *f*-photosystems**Authors:** Dennis J. Nürnberg^{1*}, Jennifer Morton², Stefano Santabarbara³, Alison Telfer¹, Pierre Joliot⁴, Laura A. Antonaru¹, Alexander H. Ruban⁵, Tanai Cardona¹, Elmars Krausz³, Alain Boussac⁶, Andrea Fantuzzi^{1*} and A. William Rutherford^{1*}**Affiliations:**¹ Department of Life Sciences, Imperial College, London SW7 2AZ, United Kingdom² Research School of Chemistry, ANU, Canberra, Australia³ Istituto di Biofisica, Consiglio Nazionale delle Ricerche, via Celoria 26, 20133 Milano, Italy⁴ Institut de Biologie Physico-Chimique, Unité Mixte de Recherche 7141 Centre National de la Recherche Scientifique-Univ P. et M. Curie, 13 rue P. et M. Curie, 75005 Paris, France⁵ School of Biological and Chemical Sciences, Queen Mary University of London, London E1 4NS, United Kingdom⁶ Institut de Biologie Intégrative de la Cellule, UMR 9198, Bât 532, CEA Saclay, 91191 Gif-sur-Yvette, France*Correspondence: a.rutherford@imperial.ac.uk; d.nurnberg@imperial.ac.uk; a.fantuzzi@imperial.ac.uk**Abstract:**

Photosystems I and II convert solar energy into the chemical energy that powers life. Both photosystems use chlorophyll-*a* photochemistry, absorbing almost the same color of light and thus accessing comparable amounts of energy. This energy is considered the “red-limit” for oxygenic photosynthesis. Here we report that a trait that is common in cyanobacteria extends the photochemical red-limit, with both photosystems using ~110 meV less energy. This ~45 nm upshift of the photochemically active chlorophylls may represent an extended red-limit relevant to stable environments. Studies of these unprecedented low-energy photosystems, with their far-red photochemistry but largely red antenna, could solve key long-standing mechanistic and energetic questions in photosynthesis, some of which are relevant to the hunt for life on planets in other solar systems. Understanding the bioenergetics and resilience of these systems could provide design principles and feasibility assessments for projects aimed at improving photosynthetic efficiency by engineering long-wavelength photosystems.

One Sentence Summary:

Long-wavelength chlorophylls in key positions in Photosystem I and II reflect an extension of the photochemical red-limit for photosynthesis.

Main Text:

Oxygenic photosynthesis uses chlorophyll-*a* (*chl_a*) to convert visible light into the chemical energy that drives the biosphere. The photochemically active pigments of the two photosystems, Photosystem II (PSII) and Photosystem I (PSI), at 680 nm and 700 nm respectively, represent the energy available for photochemistry (1–3). This was considered the “red limit” (4), the minimum energy required for oxygenic photosynthesis, until it was found that a species of cyanobacteria, *Acaryochloris marina*, extends this limit by using *chld*, a pigment that absorbs 40 nm longer than *chl_a* (5, 6). More recently *chl_f*, the longest wavelength chlorophyll known, was discovered (6–8) but it is generally assumed to play a purely light-harvesting role, needing heat for uphill excitation transfer to *chl_a* for photochemistry to occur (5, 6, 9–12) (see however (13)). Thus, in photochemical terms, this was not an extension of the red-limit.

Understanding the red-limit is also of interest to astrobiology as oxygenic photosynthesis is considered a signature for complex life and many otherwise potentially life-bearing planets are poor in visible light but rich in far-red/near infra-red light (14). Here on Earth, the poor efficiency of photosynthesis might be improved by engineering long-wavelength photosystems to extend the red-limit. Efficiency gains could be made i) by accessing the photon-rich, far-red/near-IR region of solar radiation, and ii) by cutting competition for light by making PSI and PSII use different colors (15–17). However, oxygenic photosynthesis running on less energy could lose resilience (2, 18). This concern stems from the consideration that the energy requirements contributing to the red-limit are not simply those of the energy-demanding chemistry of photosynthesis (4), but also the additional energy needed to avoid the back-reactions responsible for photo-damage (2). This debate was difficult to test as no engineered species have yet been produced and only *Acaryochloris* is known to use long-wavelength chlorophyll for photochemistry (5, 6, 10, 19, 20).

Here we have studied the photosystems in the *chl_f*-containing cyanobacterium, *Chroococcidiopsis thermalis*, when grown under far-red light. A range of biochemical and biophysical approaches provide evidence that charge separation occurs from long-wavelength chlorophylls in both photosystems. This further extension of the photochemical red-limit for is different from the singular case of *Acaryochloris*, in which both the photochemistry and main light collection is done by *chld*, which makes up more than 90% of the chlorophyll present (5, 6, 10, 19, 20). In contrast, here we report photosystems in which long-wavelength chlorophylls perform charge separation, while the vast majority of the antenna remains at short wavelength. Given the distribution of the gene cluster responsible for this trait (8, 21), this extension of the photochemical red-limit is widespread in cyanobacteria.

Photosynthetic activities at long wavelengths in cells and membranes

C. thermalis grown under far-red light (FRL) (750 nm) contains ~90% chl_a, ~10% chl_f and <1% chl_d. The absorption and fluorescence spectra of the cells were shifted towards long wavelengths with a new absorption peak at 709 nm (Fig. 1A) and 80K fluorescence at 740, 753 and 820 nm, suggesting changes in both photosystems (Fig. 1B) (see (21)). These data and decay-associated fluorescence (fig. S1) show that the FRL-chlorophylls are the dominant terminal emitters. These findings, which are comparable to those reported earlier in this and other species (8, 9, 22), indicate that long-wavelength chlorophylls are present in essentially all of the photosystems. PSI and PSII activity in FRL-cells show action spectra extending to long wavelengths, with an additional PSI peak at 745 nm and an additional PSII peak at 715 nm and these are similar to the absorption spectra of the isolated reaction centers (Fig. 1C). Figure 1D illustrates how the action spectra are manifest as photosystem activities at specific wavelengths. The effects are clear in PSI but more marked in PSII: Q_A reduction under FRL-excitation in white-light (WL) grown cells was slow and incomplete, but in FRL-cells it was very rapid, faster than in WL-cells with visible excitation (Fig. 1D lower middle panel). Q_A reduction using visible excitation was significantly slower in FRL-cells vs WL-cells (Fig. 1D middle panels), likely due to disconnected phycobilisomes in FRL-cells (23). The changes in the kinetic phases observed in FRL vs WL cells are not addressed here but presumably reflect modifications in the antenna.

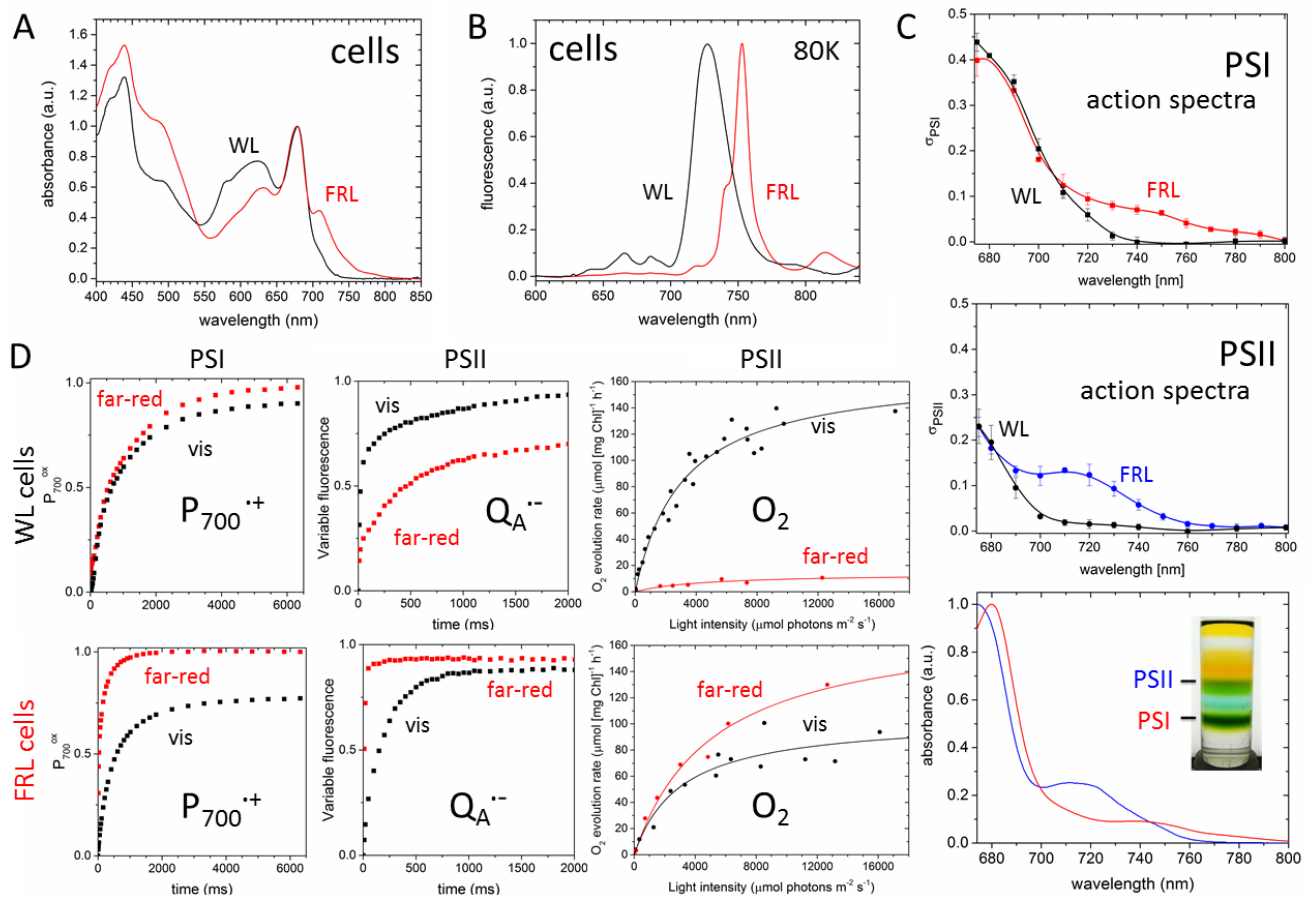


Fig. 1. Characterization of the photosystems in *C. thermalis* cells grown in white and far-red light. (A) Absorption spectra and (B) 80K fluorescence spectra of WL- and FRL-cells. (C) Action spectra (see materials and methods) for PSI (P_{700}^{*+} at 430 nm 50 μ s after the flash) (top) and PSII (Q_A^{-} +DCMU, measured as fluorescence) (middle) in FRL-cells (red and blue respectively) compared to WL-cells (black). Bottom panel: absorption spectra from isolated PSI (red) and PSII (blue); inset sucrose gradients separating the photosystems. (D) Left panels: PSI activity (P_{700}^{*+} at 705 nm 50 μ s after the flash) and middle panels: PSII activity (Q_A^{-} +DCMU, measured as fluorescence) excited by visible (520 nm) and far-red (740 nm) light using WL- (top) and FRL-cells (lower). Right panels: O_2 evolution as a function of light intensity in WL-cells (top) and FRL-cells (lower) excited with 665 nm (vis) and 750 nm (far-red) light. See materials and methods for details.

The maximum rate of O_2 evolution shown by FRL-cells under far-red illumination is similar to that seen from WL-cells under visible light (665 nm) but a higher intensity of FRL was needed reflecting the lower absorbance at 750 nm compared to 665 nm (see (8, 24) for comparable data on other species). As with Q_A reduction, when FRL-cells were illuminated with visible light, lower rates were obtained. This may be due to shading from disconnected phycobilisomes (23).

The data in Figure 1 show that all the photosystems in FRL-*C. thermalis* contain FRL-pigments that can drive their activity efficiently when excited at physiological temperatures with far-red light.

Far-red chlorophyll photochemistry in PSII

Thermoluminescence (TL) from $S_2Q_B^{-}$ (Fig. 2A) and $S_2Q_A^{-}$ (fig. S2A) (25) in FRL-thylakoids is enhanced by >25-fold compared to WL-thylakoids. TL arises from charge recombination repopulating the excited state of the primary donor chlorophyll ($*Chl_{D1}$ (26)) and emitted from there. TL intensity per recombination is mainly determined by the energy gap between the precursor charge-pair and the luminescent excited-state chlorophyll (27). The enhancement observed here, which is unprecedented in natural systems, indicates a significant decrease in that energy gap. This would occur if the primary emitter had a lower energy, i.e. a longer wavelength. Other than its enhanced-luminescence, the TL seemed relatively normal: recombination takes place at temperatures close to those seen in the WL-PSII and the flash-number dependence is nearly identical to that seen in WL-PSII, indicating no obvious change in the yields of charge separation and stabilization (fig. S2B). Thus it seems likely that there are no significant changes in critical electron transfer rates in FRL-PSII.

The rates of Q_A reduction in isolated PSII at 77K (Fig. 2B) (28) were comparable with 600 nm or 710 nm excitation when the same relative intensities were used as those that gave matching rates at 293K (Fig. 2B inset). Figure 2C shows a similar experiment using EPR to monitor PSII activity, i.e. β -carotene cation radical formation at 15K (29). Illumination at 730 nm was at least as efficient as 610 nm (see also fig. S3). If *chl*f had a pure antenna role, the energy gap between

~720 nm, the absorption of the shortest FRL-chlorophyll in FRL-PSII (see below), and the chl a PSII trap (P_{680}) would be ~100 meV; the Boltzmann energy ($k_B T$) at 293K is 26 meV but uphill exciton transfer would occur because of the overlap of the broad absorptions. However at 77K ($k_B T = 6.6$ meV) and 15K ($k_B T = 1.3$ meV) excitation transfer should be much less efficient or non-existent (30). The matching kinetics for PSII photochemistry with visible and FRL excitation at cryogenic temperatures indicate that FRL-chlorophyll is involved in primary charge separation.

Figure 2D shows difference spectra taken at 293K when the $\text{Pheo}_{D1}^{\bullet-}$ was trapped by weak illumination in the presence of a reductant (31, 32). Bleaches are present at ~546 nm and ~680 nm from $\text{Pheo}_{D1}^{\bullet-}$ and there is a blue-shift at ~669 nm, attributed to P_{D1}/P_{D2} . The $\text{Pheo}_{D1}^{\bullet-}$ -induced electrochromic blue-shift on the Chl_{D1} pigment centered at ~680 nm, which dominates the difference spectrum in WL-PSII (31, 32), is absent in the FRL-PSII. Instead the dominant feature is a blue-shift at ~725 nm. The difference spectrum obtained when FRL-PSII is illuminated at 77K (Fig. 2E) is expected to reflect Q_A reduction and ChlZ_{D2} and β -carotene oxidation (bleaches at 659 nm and 510 nm respectively). $Q_A^{\bullet-}$ causes two band-shifts on Pheo_{D1} , i) a 546 nm blue-shift (its position reflecting the presence of D1Glu130 in FRL-PSII (fig. S4)), and ii) a 685 nm red-shift. Again the expected Chl_{D1} blue-shift at ~680 nm (32) is replaced by one at ~727 nm. The band-shift data indicate that the Chl_{D1} is replaced by a FRL-chlorophyll in FRL-PSII (Fig. 2F). A small blue shift at 669 nm (P_{D1}/P_{D2}) and red-shift at 735 nm (see below) are also visible (Fig. 2E).

The TL, the low-temperature FRL photochemistry studies and the blue-shifts in the electronic absorption spectra all indicate that a FRL-chlorophyll occupies the Chl_{D1} position and is the PSII primary electron donor (Fig. 2F).

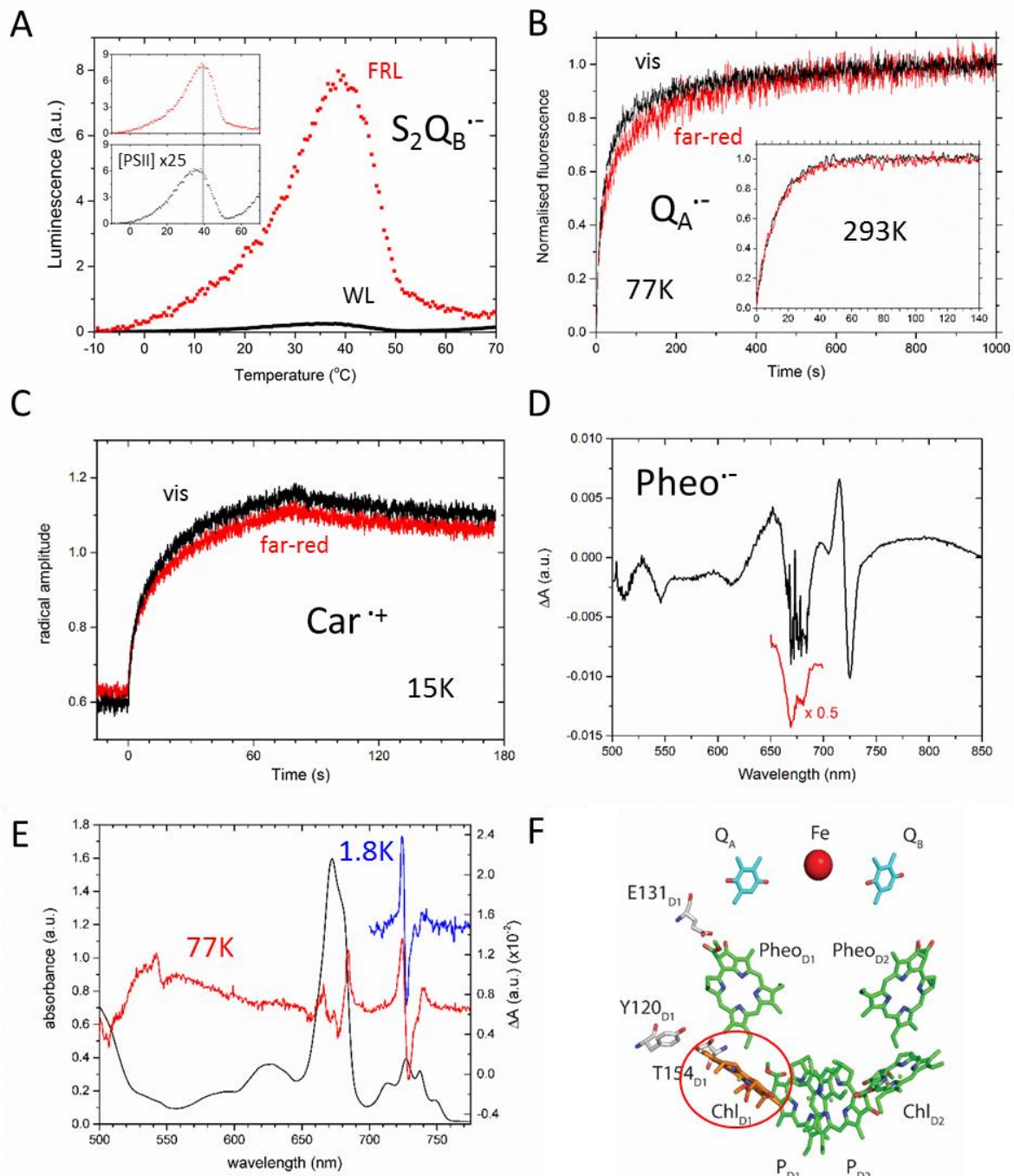


Fig. 2. FRL-PSII photochemistry. (A) $S_2Q_B^{\bullet-}$ thermoluminescence in WL- and FRL-thylakoids from *C. thermalis*. Inset: the FRL sample diluted to 25-times less PSII than in the WL-sample. (B) Kinetics of $Q_A^{\bullet-}$ reduction in FRL-thylakoids (measured as fluorescence) at 77K (inset at 293K). Samples were excited using visible (600 nm) and far-red (710 nm) light. (C) Kinetics of β -carotene cation radical formation in isolated FRL-PSII at 15K illuminated at 610 nm and 730 nm. (D) Light-minus-dark visible/near-IR spectrum at 293K upon $Pheo_{D1}^{\bullet-}$ formation in isolated FRL-PSII. The 650-700 nm region, which is saturated in the

main spectrum (black), is shown in the inset (red) from a sample diluted by 2. (E) 77K absorption spectrum of isolated FRL-PSII (black) with the 77K (red) and 1.8K (blue) illuminated–dark difference spectra after 725 nm excitation. (F) The cofactors in the core of PSII showing Chl_{D1} as a FRL-chlorophyll (orange).

PS-II FRL-chlorophyll composition and location

HPLC data on the isolated PSII indicate 4 *chl*f, 1 *chld*, 2 *phea*a and 30 *chl*a per center based on the 35 chl per PSII (33) (fig. S5A). The 77K absorption spectrum (Fig. 2E) shows 4 peaks above 700 nm. The 710 nm band is attributed to red-shifted allophycocyanins (8, 34) based on its wavelength, its variable amplitude in different preparations and the absence of MCD (fig. S6). The 1.8K absorption and MCD spectra were fitted with ~5 FRL-chl at 721, 727, 734, 736 and 749 nm (fig. S7). *Chld* absorbs at shorter wavelengths than *chl*f in solvent, it thus seems likely to be either the 721 or 727 nm pigment. The apparent requirement for a unique *chld* specific to PSII could suggest that it plays the photochemical role as the primary donor, Chl_{D1}, the 727 nm pigment. This is consistent with conserved amino acid changes near Chl_{D1} (figs. S8 and S9), indicating specific H-bonding to the formyl group on *chld*, and is supported by the fact that *chld* (with the same conserved H-bonding residues) plays this role in *Acaryochloris* (19, 20). It is just as likely that *chl*f is in this position as the H-bonding changes are also consistent with the presence of *chl*f (fig. S9).

The 721 nm chl could play a role as a linker between the trap and the *chl*a antenna and is thus another potential location for the *chld* (see below). The 3 remaining long-wavelength chlorophylls appear to be tuned to span the energy gap from 749 nm up to the photochemical trap at 727 nm, with gaps of 10-12 nm (23-26 meV), appropriate for the heat in the environment ($k_B T = 26$ meV) to allow efficient exciton transfer at growth temperatures. This will likely be reflected in their locations, with the four FRL-antenna chlorophylls arranged in a short chain/network with the distal 749 nm *chl*f connected to the 727 nm trap via the chlorophylls of intermediate wavelengths. This chain of FRL-antenna will accept excitation from the 30 *chl*a and phycocyanobilin antenna. The excitation wavelength dependence of the 77K fluorescence in isolated PSII confirms that all the *chl*a molecules are connected to *chl*f with the dominant emission at 755 nm with all excitation wavelengths from 590 nm to 745 nm (fig. S10).

The light-dark difference spectrum (Fig. 2E) also shows a red-shift at 736 nm. From the orientation and distances between cofactors in the *T. vulcanus* structure, there are several possible candidates: Chl_{D2}, Chl508 and Chl612 (fig. S11). Chl508 is the closest non-core chlorophyll to Chl_{D1} linking the CP43 antenna to the 6 photochemical core chlorins. Chl612 is the CP47 symmetrical counterpart of Chl508. Both Chl508 and Chl612 are closer to Q_A⁻ than is Chl_{D2} and the Chl612 is the best oriented to give a red-shift. The Chl612 has already been suggested to undergo a similar red shift in *chl*a-containing PSII (35). From these arguments Chl612 is the best candidate for the 736 nm *chl*f but we do not rule the other two. In functional

terms it appears quite attractive for Chl508 and Chl612, the symmetrical antenna-to-core linkers, to be FRL-pigments. It seems possible that the Chl508 (perhaps the 721 nm chl), on the CP43 side connects to the chl*a* antenna.

We have little relevant data on the pigments at 734 and 749 nm. From the fluorescence study (fig. S10) showing 755 nm emission (presumably from the 749 nm chl) dominating at all temperatures, the simplest model would be to have the 734 and 749 nm pigments close to each other (the Chl611 and Chl602 perhaps) and delivering excitation to the same linker (the Chl612 at 736 nm). Several other options exist but further data is required before good assignments can be made.

It seems likely that P_{D1}, which bears the cation radical that oxidizes the redox tyrosine, Tyr_z, remains a chl*a*. This is based on i) the presence of the blue-shifts at 669 nm (Fig. 2D and E), ii) structural considerations (figs. S8 and S12), iii) the precedence of chl*a* being P_{D1} in *Acaryochloris* (5, 6, 19, 20) and iv) conservation of appropriate chemical properties (e.g. oxidizing power, stability and reactivity) without the need for major redox and kinetic tuning. Sequence comparisons indicate changes in the environments of key cofactors in the redox core (figs. S9, S12 and S13) and in the antenna (fig. S14) of FRL-PSII, consistent with the redox and energy (color) tuning needed to function in FRL.

PSI chlorophyll *f* photochemistry

Excitation of FRL-PSI at 15K using 610, 730 and 750 nm light gave comparable photochemistry (Fig. 3A and fig. S15), indicating that the chlorophyll absorbing at ~750 nm is involved in charge separation. In WL-PSI 750 nm illumination at 15K resulted in low quantum yield photochemistry as expected (30, 36, 37).

The light-minus-dark difference spectra at 293K in FRL- and WL-thylakoids corresponds well with those obtained at 77K and 1.8K from isolated FRL- and WL-PSI after taking into account the narrowing of the bands (Fig. 3B and fig. S16). The main bleach is at ~704 nm with an absorption increase at 692 nm, indicating that the cation is shared on the P₇₀₀ chlorophyll *a/a'* pair, as seen in the WL-PSI. The rest of the spectrum shows marked differences: the sharp trough at 684 nm, the peak at 674 nm (680 nm at 77K) and the trough at 656 nm (~660 nm at 77K), which are present in WL-PSI (Fig. 3B and fig. S16) are all absent in FRL-PSI. Instead several changes appear at >700 nm (Fig. 3B). These changes can be attributed to the replacement of chl*a* band-shifts in WL-PSI with chl*f* band-shifts in FRL-PSI. The band-shifts >700 nm are better resolved at 77K and 1.8K and show a broad blue-shift (or two overlapping blue-shifts) at ~745 nm, a sharp red-shift at 756 nm and a weak blue-shift at 800 nm. In addition, there is a red-shift at ~681 nm, which is likely present but obscured in WL-PSI.

FRL-PSI chlorophyll-*f* composition and location

From HPLC FRL-PSI contains 7-8 *chl_f*, 0 *ch_ld*, 0 *pheo* and ~88-89 *chl_a* (fig. S5B) assuming 96 *chl* per PSI (36). The 1.8K absorption and MCD spectra at >700 nm can be fitted as follows, 1 *chl_f* at 736 nm, 3 *chl_f* at ~745 nm, 1 *chl_f* at 756 nm, 1 *chl_f* at ~763 nm and ~2*chl_f* at ~800 nm (fig. S18). In addition a chlorophyll at 709 nm is present and is suggested to be a long-wavelength PSI *chl_a*.

Based on the crystal structure of PSI (38), the difference spectra (Fig. 3B, fig. S16), the low temperature photochemistry (Fig. 3A and fig. S15) and structural arguments (figs. S8 and S19), we suggest the following model for the FRL-PSI redox cofactors: i) P_A and P_B remain *chl_a* and bear the P_{700} cation. ii) A_{0A} and A_{0B} , the primary acceptors (3, 39), remain *chl_a*, since the redox properties of *chl_f* (12) make it unsuitable for such a low potential role. This fits with the assignment of the red-shift at ~684 nm to A_0 (Fig. 3B see (39)) and with A_0 being *chl_a*, in *Acaryochloris* (20). iii) One or both of the primary donors, A_{-1A} and A_{-1B} , (40), are *chl_f* in FRL-PSI, absorbing at ~745 nm. They give the (overlapping?) blue-shifts at this wavelength, replacing the dominant ~684 nm blue-shift in the WL-PSI. A_{-1A} and A_{-1B} are the only redox active chlorophylls oriented to allow a blue-shift.

Assuming a total of 8 *chl_f*, the remaining 6 *chl_f* molecules must play antenna roles but with ~90 possible locations, they are harder to place. The absorption spectra and the chemical properties do allow some suggestions. The primary donors (A_{-1}) at ~745 nm are likely to be connected to the longer wavelength antenna via *chl_f* molecules with intermediate wavelengths to allow efficient exciton transfer at room temperature. Thus the 756 nm *chl_f* may link longer wavelength antenna to the 745 nm A_{-1} . The 756 nm band is the narrowest of the absorptions and the CD and MCD show it is only weakly coupled to other chlorophylls. The linkers, ChlA40 and ChlB39, are good candidates for the 756 nm *chl_f*, being i) between the antenna and the redox cofactors and not intimately connected to either group (41) ii) correctly oriented for the observed red-shift, and iii) within 15Å from P_{700}^{*+} (see fig. S19). Given there is only one *chl_f* under this narrow peak, this implies asymmetry but ChlA40 and ChlB39 are equally likely candidates.

The position of the 800 nm peak shifts with temperature, resolves into two sub-peaks (794 and 802 nm) and has CD and MCD properties (fig. S17) typical of the charge transfer character expected from an electronically coupled *chl_f* dimer, the FRL equivalent of the “red chlorophylls” in WL-PSI (42). This dimer also acts as the terminal emitter at 815 nm (fig. S10). There are several candidate chlorophyll dimers (38, 41). We consider ChlA38/ChlA39 (or ChlB37/ChlB38) as candidates as they are located (~10Å) from the ChlA40 (or ChlB39) linkers and distal from the redox core, close to the stromal surface. They are closer (~28Å) to P_{700}^{*+} than most of the other candidate dimers and even closer to F_A^- (the reduced Fe_4S_4 electron acceptor (3)) and so seem good candidates for the observed band-shift. The shorter distance

between F_A^- and ChlB37/ChlB38 ($\sim 26\text{\AA}$) compared to the A-side counterparts ($\sim 30\text{\AA}$) could favor the B-side option. Further evidence is required to assign these and the remaining chl*f* more firmly.

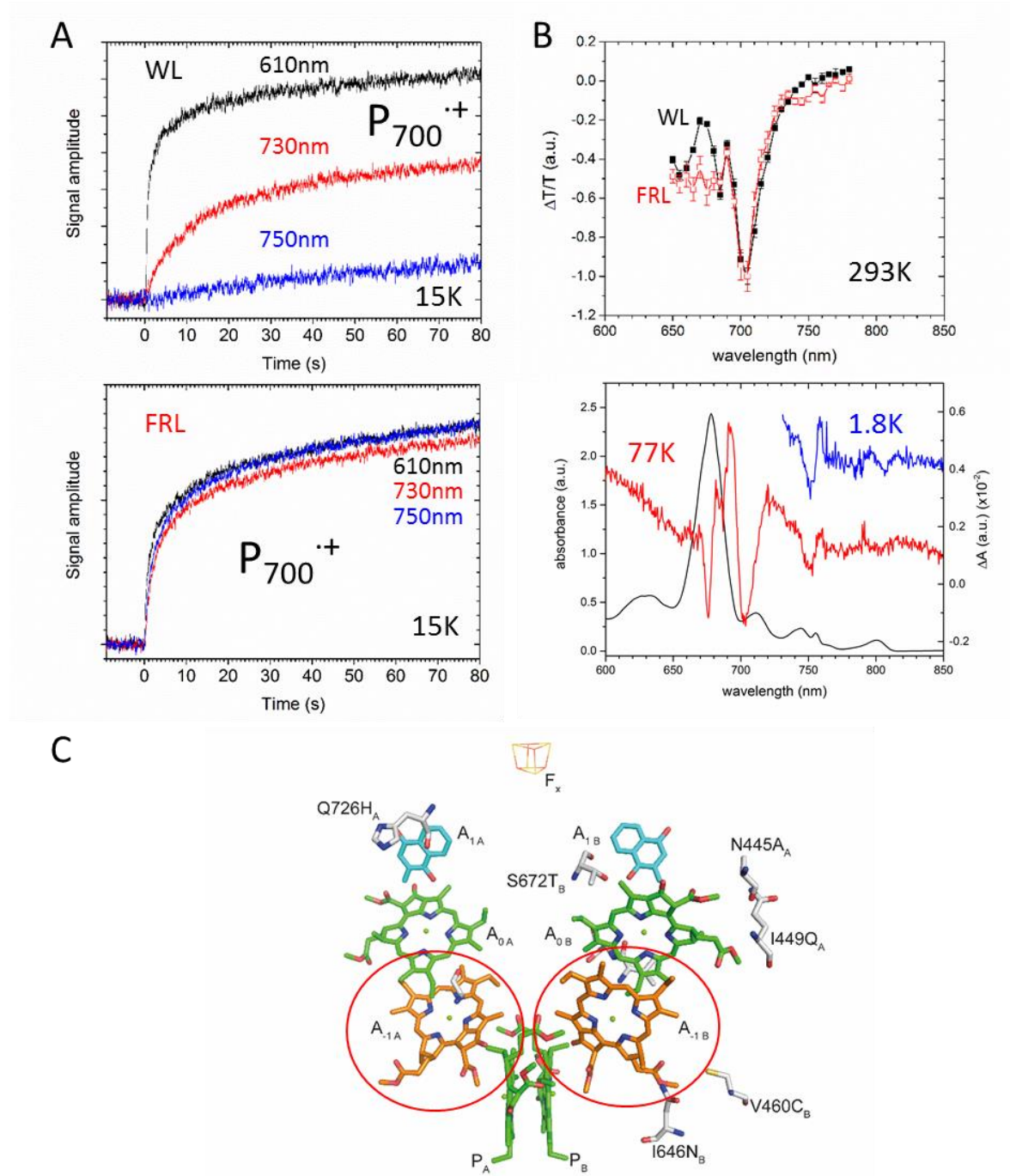


Fig. 3. FRL-PSI Photochemistry. (A) Low temperature (15K) photo-accumulation of $P_{700}^{\cdot+}$ monitored by EPR using visible and far-red light at the wavelengths noted. Upper panel isolated WL-PSI, lower panel

isolated FRL-PSI. (B) Upper panel, flash-induced P_{700}^{++} 293K absorption difference spectrum using FR- and WL-thylakoids. Lower panel, P_{700}^{++} 77K (red) and 1.8K (blue) difference spectrum using isolated FRL-PSI and 1.8K absorption spectrum (black). (C) FRL-PSI model showing conserved amino acid changes PSI from the FarLiP cluster. Red circles show the proposed locations of *chl*f (orange) with other chl assumed to be *chl*a (see text).

Discussion

Despite having *chl*f that can absorb at >760 nm available for FRL-PSII photochemistry, the wavelength used for the primary electron donor is ~ 727 nm (fig. S20). This is very similar to the primary donor in *Acaryochloris* PSII, the *chl*d-containing species (6, 19, 20). Thus both of the known cases of PSII functioning “beyond the red-limit” seem to use the same wavelength (and possibly the same pigment). This may not be a coincidence; it may represent a second red-limit for PSII, one that applies when functioning in a stable-light, deep-shade environment. The energy sacrificed by the shift from ~ 680 nm to 727 nm may represent the energy headroom needed by PSII to mitigate the photodamage caused by variable light intensities (2, 18) due to pulses of electric field, $\Delta\Psi$, which favor harmful back-reactions (43). This second red-limit should apply to FRL-PSII in other far-red cyanobacterial species growing in comparable, stable conditions.

Other than the primary donors, Chl_{D1} and A-1, the other redox cofactors in PSII and PSI appear to remain the same, however they must be tuned to account for the decrease in energy. The ~ 110 meV energy shortfall may be distributed among the electron transfer steps occurring on each photochemical turnover. The enhanced-luminescence in FRL-PSII reported here reflects a decrease in the driving force for the charge-separation step, but it is likely that the most significant functional difference will be a decrease in the biggest energy gap, that between the Phe_{OD1} and Q_A , which controls its back-reaction route (2). If so, while this is expected to have little effect on forward electron transfer, it will favor photodamage from back-reactions (2). This should not be a problem under the stable, shaded conditions associated with FRL-growth in nature. Future studies will focus on investigating redox tuning, energetics and susceptibility to photodamage.

The FRL-photosystems maintain the energy difference between their two primary reactions that exists in WL; this too is probably significant (fig. S20). If it were advantageous to separate the two photosystems to avoid competition for light, as suggested (15–17), species like that studied here would do so under normal light with *chl*a-PSII and *chl*f-PSI. This does not appear to occur. This may reflect the need for the two photosystems working in series to have essentially the same rate of excitation and thus comparable turnover rates, or at least rates that are similar enough to allow appropriate regulation, thereby avoiding either one of the photosystems out-running the other and the consequent photodamage. The present work indicates that the red-limit can be extended for PSII but only by ~ 110 meV and while PSI may in principle function at lower

energies without incurring too much photodamage, it is tied to the PSII red-limit by the need for the two sequential photosystems to run at similar rates.

References and Notes:

1. H. Dau, I. Zaharieva, Principles, efficiency, and blueprint character of solar-energy conversion in photosynthetic water oxidation. *Acc Chem Res.* **42**, 1861–1870 (2009).
2. A. W. Rutherford, A. Osyczka, F. Rappaport, Back-reactions, short-circuits, leaks and other energy wasteful reactions in biological electron transfer: Redox tuning to survive life in O₂. *FEBS Lett.* **586**, 603–616 (2012).
3. J. H. Golbeck, Ed., *Photosystem I. The Light-driven Plastocyanin:Ferredoxin Oxidoreductase* (Springer Netherlands, 2006).
4. L. O. Björn, G. C. Papageorgiou, R. E. Blankenship, Govindjee, A viewpoint: Why chlorophyll a? *Photosynth Res.* **99**, 85–98 (2009).
5. P. Loughlin, Y. Lin, M. Chen, Chlorophyll d and *Acaryochloris marina*: current status. *Photosynth Res.* **116**, 277–293 (2013).
6. H. Miyashita *et al.*, Discovery of Chlorophyll d in *Acaryochloris marina* and Chlorophyll f in a Unicellular Cyanobacterium, Strain KC1, Isolated from Lake Biwa. *J Phys Chem Biophys.* **4**, 149 (2014).
7. M. Chen, A Red-Shifted Chlorophyll. *Science.* **329**, 1318–1319 (2010).
8. F. Gan *et al.*, Extensive remodeling of a cyanobacterial photosynthetic apparatus in far-red light. *Science.* **345**, 1312–1317 (2014).
9. S. Itoh *et al.*, Harvesting Far-Red Light by Chlorophyll f in Photosystems I and II of Unicellular Cyanobacterium strain KC1. *Plant Cell Physiol.* **56**, 2024–2034 (2015).
10. S. I. Allakhverdiev *et al.*, Chlorophylls d and f and their role in primary photosynthetic processes of cyanobacteria. *Biochem.* **81**, 201–212 (2016).
11. D. M. Niedzwiedzki, H. Liu, M. Chen, R. E. Blankenship, Excited state properties of chlorophyll f in organic solvents at ambient and cryogenic temperatures. *Photosynth Res.* **121**, 25–34 (2014).
12. M. Kobayashi *et al.*, in *Photosynthesis*, Z. Dubinsky, Ed. (InTech, 2013).
13. M. Kaucikas, D. J. Nürnberg, G. Dorlhac, A. W. Rutherford, J. Van Thor, Femtosecond Visible Transient Absorption Spectroscopy of Chlorophyll f-Containing Photosystem I. *Biophys J.* **112**, 234–249 (2017).
14. R. D. Wolstencroft, Photosynthesis: Likelihood of Occurrence and Possibility of Detection on Earth-like Planets. *Icarus.* **157**, 535–548 (2002).
15. R. E. Blankenship *et al.*, Comparing Photosynthetic and Photovoltaic Efficiencies and Recognizing the Potential for Improvement. *Science.* **332**, 805–809 (2011).
16. D. R. Ort *et al.*, Redesigning photosynthesis to sustainably meet global food and bioenergy demand. *Proc Natl Acad Sci USA.* **112**, 8529–8536 (2015).
17. R. Croce, H. van Amerongen, Natural strategies for photosynthetic light harvesting. *Nat. Chem. Biol.* **10**, 492–501 (2014).
18. C. A. R. Cotton *et al.*, Photosynthetic constraints on fuel from microbes. *Front. Bioeng.*

- Biotechnol.* **3**, 1–5 (2015).
19. T. Renger, E. Schlodder, The Primary Electron Donor of Photosystem II of the Cyanobacterium *Acaryochloris marina* Is a Chlorophyll d and the Water Oxidation Is Driven by a Chlorophyll a/Chlorophyll d Heterodimer. *J Phys Chem B.* **112**, 7351–7354 (2008).
 20. S. Itoh *et al.*, Function of Chlorophyll d in Reaction Centers of Photosystems I and II of the Oxygenic Photosynthesis of *Acaryochloris marina*. *Biochem.* **46**, 12473–12481 (2007).
 21. C. Zhao, F. Gan, G. Shen, D. A. Bryant, RfpA, RfpB, and RfpC are the master control elements of far-red light photoacclimation (FaRLiP). *Front. Microbiol.* **6**, 1–13 (2015).
 22. M. Chen, Y. Q. Li, D. Birch, R. D. Willows, A cyanobacterium that contains chlorophyll f - a red-absorbing photopigment. *FEBS Lett.* **586**, 3249–3254 (2012).
 23. E. L.-W. Majumder *et al.*, Subcellular pigment distribution is altered under far-red light acclimation in cyanobacteria that contain chlorophyll f. *Photosynth Res* (2017), doi:10.1007/s11120-017-0428-1.
 24. Y. Li, Y. Lin, P. C. Loughlin, M. Chen, Optimization and effects of different culture conditions on growth of *Halomicronema hongdechloris* – a filamentous cyanobacterium containing chlorophyll f. *Front Plant Sci.* **5**, 1–12 (2014).
 25. A. W. Rutherford, A. R. Crofts, Y. Inoue, Thermoluminescence as a probe of Photosystem II photochemistry. The origin of the flash-induced glow peaks. *Biochim Biophys Acta.* **682**, 457–465 (1982).
 26. B. A. Diner, F. Rappaport, Structure, dynamics, and energetics of the primary photochemistry of Photosystem II of oxygenic photosynthesis. *Annu Rev Plant Biol.* **53**, 551–580 (2002).
 27. F. Rappaport, J. Lavergne, Thermoluminescence: theory. *Photosynth Res.* **101**, 205–216 (2009).
 28. W. W. I. Adams, B. Demmig-Adams, K. Winter, U. Schreiber, The ratio of variable to maximum chlorophyll fluorescence from photosystem II, measured in leaves at ambient temperature and at 77K, as an indicator of the photon yield of photosynthesis. *Planta.* **180**, 166–174 (1990).
 29. J. Hanley, Y. Deligiannakis, A. Pascal, P. Faller, A. W. Rutherford, Carotenoid Oxidation in Photosystem II. *Biochemistry.* **38**, 8189–8195 (1999).
 30. E. Schlodder *et al.*, Long-Wavelength Limit of Photochemical Energy Conversion in Photosystem I. *J Am Chem Soc.* **136**, 3904–3918 (2014).
 31. V. V. Klimov, A. V. Klevanik, V. A. Shuvalov, Reduction of pheophytin in the primary light reaction of Photosystem II. *FEBS Lett.* **82**, 183–186 (1977).
 32. N. Cox *et al.*, Identification of the Q Y Excitation of the Primary Electron Acceptor of Photosystem II: CD Determination of Its Coupling Environment. *J Phys Chem B.* **113**, 12364–12374 (2009).
 33. Y. Umena, K. Kawakami, J.-R. Shen, N. Kamiya, Crystal structure of oxygen-evolving photosystem II at a resolution of 1.9 Å. *Nature.* **473**, 55–60 (2011).
 34. Y. Li *et al.*, Characterization of red-shifted phycobilisomes isolated from the chlorophyll f-containing cyanobacterium *Halomicronema hongdechloris*. *BBA - Bioenerg.* **1857**, 107–

114 (2016).

35. J. L. Hughes, E. Krausz, Novel characteristics of persistent spectral hole-burning and hole-filling in Photosystem II core complexes. *J Lumin.* **127**, 239–244 (2007).
36. J. R. Reimers *et al.*, Challenges facing an understanding of the nature of low-energy excited states in photosynthesis. *Biochim Biophys Acta.* **1857**, 1627–1640 (2016).
37. F. Mokvist, F. Mamedov, S. Styring, Defining the Far-red Limit of Photosystem I: The primary charge separation is functional to 840 nm. *J Biol Chem.* **289**, 24630–24639 (2014).
38. P. Jordan *et al.*, Three-dimensional structure of cyanobacterial photosystem I at 2.5 Å resolution. *Nature.* **411**, 909–917 (2001).
39. A. Chauvet, N. Dashdorj, J. H. Golbeck, T. W. Johnson, S. Savikhin, Spectral Resolution of the Primary Electron Acceptor A0 in Photosystem I. *J Phys Chem B.* **116**, 3380–3386 (2012).
40. M. G. Müller, C. Slavov, R. Luthra, K. E. Redding, A. R. Holzwarth, Independent initiation of primary electron transfer in the two branches of the photosystem I reaction center. *Proc Natl Acad Sci USA.* **107**, 4123–4128 (2010).
41. M. Byrdin *et al.*, Light harvesting in photosystem I: Modeling based on the 2.5-Å structure of photosystem I from *Synechococcus elongatus*. *Biophys J.* **83**, 433–457 (2002).
42. N. V Karapetyan *et al.*, Long Wavelength Chlorophylls in Photosystem I of Cyanobacteria : Origin , Localization , and Functions. *Biochem.* **79**, 213–220 (2014).
43. G. A. Davis *et al.*, Limitations to photosynthesis by proton motive force-induced photosystem II photodamage. *Elife*, 1–27 (2016).

Acknowledgments:

We dedicate this work to our friend and colleague Fabrice Rappaport, who died in January 2016, with whom we worked in the early stages of this project. This work was supported by BBSRC grants BB/L011506/1, BB/R001383/1, a Leverhulme Trust grant RPG-2017-223 and a Wolfson Merit Award from the Royal Society to A.W.R., an Australian Research Council grant DP150103137 to E.K., an Imperial College London Junior Research Fellowship to TC. We thank J. W. Murray for discussions, B. Nwaobi for technical support, C. Mullineaux for access to a 77K fluorimeter for initial measurements and B. Bailleul and W. Remelli for technical help in obtaining the absorption spectra. We thank J.-M. Ducruet for lending us the thermoluminescence set-up and L. Haigh for her assistance with the HPLC analysis.

Supplementary Materials:

Materials and Methods

Figures S1-S20

References



Supplementary Materials for

Photochemistry beyond the red-limit in chlorophyll *f*-photosystems

Dennis J. Nürnberg, Jennifer Morton, Stefano Santabarbara, Alison Telfer, Pierre Joliot, Laura A. Antonaru, Alexander H. Ruban, Tanai Cardona, Elmars Krausz, Alain Boussac, Andrea Fantuzzi and A. William Rutherford

correspondence to: a.rutherford@imperial.ac.uk, d.nurnberg@imperial.ac.uk,
a.fantuzzi@imperial.ac.uk

This PDF file includes:

Materials and Methods
Figs. S1 to S20

Materials and Methods

Culture conditions

Cells of *Chroococcidiopsis thermalis* PCC 7203 were grown in liquid BG11 medium (1) at 30°C to OD₇₈₀ = 0.4-0.6. For whole cell experiments 100 ml cultures were grown in 250 ml Erlenmeyer flasks shaken at 110 rpm. For thylakoid preparations cells were cultured in 10 l bottles bubbled with sterile air and stirred every 24 h. Two light conditions were used: white light of ~30 $\mu\text{mol photons m}^{-2} \text{ s}^{-1}$ (Quantitherm light meter, Hansatech) and far-red light (750 nm, Epitex; L750-01AU) of ~30 $\mu\text{mol photons m}^{-2} \text{ s}^{-1}$ (optical power meter, Newport).

Oxygen evolution measurements

Oxygen evolution rates for cells of *C. thermalis* grown in WL and FRL were measured with a Clark-type electrode (Oxygraph, Hansatech) at 25°C. Samples were adjusted to a total chlorophyll concentration of 28-44 $\mu\text{g chl ml}^{-1}$ and kept in the dark for >10 min. 1 mM DCBQ (2,5-Dichloro-1,4-benzoquinone) and 2 mM ferricyanide were used as an electron acceptor system. For illumination lab-built dimmable LED lights with a peak wavelength at 665 nm and 745 nm were used. When required the excitation light intensity was reduced by using neutral density filters (Thorlabs). Light intensities were measured with a Newport Power Meter 1918-C at the respective LED wavelengths.

Isolation of thylakoid membranes and photosynthetic complexes

Cells were harvested by centrifugation at 3,000 x g for 3 min and resuspended in ice-cold buffer A (50 mM MES-NaOH pH 6.5, 5 mM CaCl₂, and 10 mM MgCl₂) with a protease inhibitor mixture (1 mM aminocaproic acid, 1 mM benzamidine, and 0.2 % (w/v) bovine serum albumin) and 0.5 mg ml⁻¹ DNase. All following steps were performed on ice under dim green light. Cells were broken by two passages through a cell disruptor (Constant System, Model T5) at a pressure of 25 kPsi. Unbroken cells were removed by centrifugation for 5 min at 3,000 x g and 4°C. Thylakoid membranes were pelleted by centrifugation at 125,000 x g and 4°C for 60 min and washed three times with buffer A. Membranes were resuspended in buffer A to a final chlorophyll concentration of 0.4 mg ml⁻¹. The amount of total chlorophyll was determined according to (2). For solubilization 0.4 % (w/v) n-dodecyl- β -maltoside (DM) was added and the suspension was incubated for 60 min at 4 °C under constant stirring. Non-solubilized material was removed by centrifugation (35 min, 22,000 x g, 4°C). Photosynthetic complexes were separated on sucrose density gradients prepared by the freeze-thawing technique (3). Centrifuge tubes were filled with buffer A containing 0.5 M sucrose and 0.04 % (w/v) DM, frozen at -20°C and thawed at room temperature. Solubilized material was loaded onto the gradients and centrifuged for 16 h at 4°C and 110,000 x g. Fractions were removed from the sucrose gradients and concentrated using centrifugal filter units (Merck, 100 kDa MWCO). Further

purification was done by anion exchange chromatography using a Mono Q 5/50 GL column (GE Healthcare). The column was equilibrated with 20 mM MES-NaOH pH 6.5 and 0.03% (w/v) DM and a linear gradient of NaCl from 0 to 0.6 M in 45 min with a flow rate of 0.5 ml min⁻¹. Fractions were analyzed by absorption spectroscopy and concentrated as mentioned above. Samples were frozen in liquid nitrogen and stored at -80°C.

HPLC detection of pigments

Reverse phase HPLC was used to demonstrate the presence of *chl*f** and *chl*d** in purified PSI and PSII. Pigments were extracted into ice-cold 100% (v/v) methanol, passed through a 0.2 µm syringe filter and loaded on a Spherisorb ODS2 column (80 Å, 3 µm, 125 x 4.6 mm, Waters) connected to an UltiMate 3000 UHPLC system (Thermo Fisher Scientific). For elution, a mobile phase gradient based on ammonium acetate, methanol, acetonitrile and ethyl acetate was used as previously described in method C in (4). The ratios of chlorophylls were calculated based on the peak intensity and their extinction coefficient at the assigned wavelengths: 71.43 mM⁻¹ cm⁻¹ for *chl*a** at 665 nm (4), 53.97 mM⁻¹ cm⁻¹ for *pheo*a** at 665 nm (5), 63.68 mM⁻¹ cm⁻¹ for *chl*d** at 697 nm and 71.11 mM⁻¹ cm⁻¹ for *chl*f** at 707 nm (6). A total number of 37 chlorins (35 chlorophylls and 2 pheophytins) per PSII was assumed for the PSII from *C. thermalis* based on the crystal structure of PSII from *Thermosynechococcus vulcanus* (7) and 96 chlorophylls per PSI based on the crystal structure from *Thermosynechococcus elongatus* (8).

PSII Photochemistry: Thermoluminescence

Thermoluminescence (TL) was measured with a lab-built apparatus, essentially as described by (9) but using the GaAsP photomultiplier H10769A-50 (Hamamatsu) with high sensitivity in the near-infrared. Samples of *C. thermalis* thylakoids (in buffer A) were normalized to the same amount of active PSII by measuring oxygen evolution using a Clark-type electrode (Oxygraph, Hansatech) at 30°C, illuminating the sample with a saturating concentration of photons of either red light ($\lambda_{\text{max}} = 665$ nm) for the WL-grown samples or far-red light ($\lambda_{\text{max}} = 745$ nm) for the FRL-grown sample and considering the total chlorophyll concentration, determined as described by (2). The samples were pre-illuminated with room light (~ 20 µmol m⁻² s⁻¹) for 30 s, dark-adapted for 5 min and then cooled to 5°C. After 2 min, the samples were excited with a single turnover saturating flash or with multiple flashes when indicated. The samples were then rapidly cooled to -15°C and luminescence was recorded with a 20°C min⁻¹ heating rate.

PSI and PSII Photochemistry at 15K: EPR (Figs 2C, 3A, figs. S3, S15)

Electron Paramagnetic Resonance (EPR) spectra were recorded using an Elexsys 500 X-band spectrometer equipped with an ER 4102 X-band resonator (Bruker), an ESR 900 cryostat and an ICT504 temperature controller (Oxford Instruments). Instrument settings

were as follows: microwave frequency, 9.49 GHz; modulation frequency, 100 kHz. Other settings were as indicated in the figure legends.

Isolated PSII (~1 mg chlorophyll ml⁻¹) were loaded in the dark into quartz EPR tubes with an inner diameter of 3 mm, dark-adapted for 30 min and frozen in a solid CO₂/ethanol bath at 200K. Isolated PSI samples (~1 mg chlorophyll ml⁻¹) were incubated with 0.5 mM ascorbate, 10 μM phenazine methosulfate (PMS) and 10 μM 2,6-dichlorophenolindophenol (DCPIP) for 5 min before freezing. Samples were degassed by pumping (~10⁻³ bar) at 200K, filled with helium gas and the EPR tubes were then transferred into liquid nitrogen. All sample handling was done in darkness.

Samples were illuminated using a low-voltage halogen lamp (24V, 250W, Philips Type 13163) and when indicated band-pass/laser-line filters at 610 nm (10BPF10-610, Newport), 730 nm (FL730-10, Thorlabs) and 750 nm (10BPF10-750, Newport) were used. The emission spectra showing the relative light intensities of these filters are shown in figures S3A and S15A along with the absorption spectra of the isolated PSII and PSI respectively.

Absorption spectroscopy

1) PSII: Pheophytin trapping at room temperature (Fig. 2D)

Photoinduced reduction of the Phe_{OD1} in the presence of Q_A^{•-} was performed similar to (10). Q_A was reduced by adding stoichiometric amounts of sodium dithionite to a degassed solution of isolated PSII (~5 μg chlorophyll ml⁻¹ in buffer A + 0.03% (w/v) DM) in a sealed cuvette. Samples were then illuminated for 1 min at room temperature with red light from a 150 W halogen lamp (590 nm long-pass filter; ~200 μmol photons m⁻² s⁻¹). Spectra, before and after illumination, were recorded with a diode array spectrophotometer, HP 8453. A 450 nm long-pass filter was used to reduce the intensity of the measuring light. Samples were allowed to relax in the dark for 15 min before repeating the illumination step.

2) PSI: P₇₀₀ oxidation kinetics at room temperature (Fig. 1D)

The rate of P₇₀₀ oxidation was determined in *C. thermalis* cells (10 μg chlorophyll ml⁻¹) in the presence of 20 μM 3-(3,4-dichlorophenyl)-1,1-dimethylurea (DCMU) using a JTS-10 spectrophotometer (Bio-Logic) by measuring the absorption changes at 705 nm using short detection flashes of 12 μs duration (11). Green and far-red actinic illumination was provided by LEDs at 520 nm (700 μmol photons m⁻² s⁻¹) and 740 nm (1700 μmol photons m⁻² s⁻¹), respectively (12). The intensity of the two actinic illuminations was set empirically so as to obtain similar PSI photochemical rates in the WL cells. The P₇₀₀ kinetics were normalized to the maximum signal (P₇₀₀ max). The DCMU was always present to prevent electron flow from PSII to PSI.

3) PSI and PSII spectroscopy measurements at low temperature

(Figs. 2E, 3B, figures S6, S7, S10, S16, S17, S18)

For the Magnetic Circular Dichroism (MCD) spectra and the majority of the low temperature absorption spectroscopy the laboratory-constructed spectrometer described in (13) was used. The system includes a 0.75M Spex monochromator and an Oxford Instruments SM-4 magnet cryostat. All absorption measurements used the same 240W halogen lamp as the light source.

Absorption and CD were measured with a Hamamatsu R669 photomultiplier in the range of 420-850 nm. For absorption spectra a 420-nm cut-off filter was used for the wide scans and a 660-nm filter used when measuring the >700-nm region in detail. Repeated scans before illumination showed no detectable actinic effects at the measuring light level used. To measure the MCD a windowless 5 mm Advanced Photonix silicon avalanche diode was used. MCD spectra were measured at 1.8 K and 5 T. Samples were illuminated prior to the measurement to reduce further actinic effects during the course of the measurements.

The samples were loaded under low light into titanium quartz cells of 500 μm , 200 μm or 50 μm pathlength. The cryoprotectant glycerol/ethylene glycol (1:1) was added to the samples to a final concentration of 45 % (v/v). Isolated PSII samples were dark-adapted for 5 min before being rapidly cooled in either liquid nitrogen or helium. Purified PSI samples were treated with 5 mM sodium ascorbate and 10 μM PMS and incubated for 30 min in the dark before the measurements.

The PSI difference spectra in fig. S16 were recorded in a laboratory-assembled set-up using a liquid nitrogen cooled CCD detector (Princeton Applied Research) coupled to a spectrograph (Acton Research Co., SpectraPro-300i) as previously described by (14). The light (440 nm) was attenuated by a combination of neutral density filters (Balzers) and a broad-band cut-on filter (Schott, OG550) to minimize actinic effects of the measuring light. In these experiments isolated PSI samples were dark-adapted in the presence of 5 mM ascorbate in 60 % (v/v) glycerol, cooled to 80K and illuminated for 10 min. The difference spectra were then calculated.

4) PSI: Time-resolved optical spectroscopy at room temperature

a) Figure 3B. The light-induced difference absorption spectra of PSI were measured in thylakoids at 293K in the presence of 20 μM DCMU and 2 mM hydroxylamine using lab-built pump-probe set-ups, with microsecond resolution as previously described with minor modifications (15). Both the pump and the probe pulse were provided by a Xe flash lamp, with the delay set by a computer-programmable lab-built pulse sequencer. The temporal resolution of the instrument was $\sim 5 \mu\text{s}$. The actinic flash wavelength was selected by a combination of two BG38 (Schott) cut-off filters. The probe wavelength was selected using

a monochromator, with a bandwidth of 2 nm (FWHM). The detecting photodiodes were protected by a combination of cut-on filters, OG550 and RG620 (Schott). The difference absorption was recorded at selected pump-probe delay times. The time traces acquired in the 600-800 nm window were analyzed in terms of a sum of exponential decay functions, using a global fitting procedure as previously described (16). The fit outcomes yield the decay lifetimes and the respective decay associated spectra.

b) Figure 1C. The PSI action spectra were measured with a lab-built set-up that works in the nanosecond-to-microsecond time-regime as previously described (17). The out-put of two optical parametric oscillators (OPO), each pumped by a separate frequency trebled Nd:YAG lasers (Coherent), provided the pump and probe pulses. The temporal resolution of the system was ~2 ns. The use of an Nd:YAG pumped OPO as a pump-source allows for almost continuous tuning of the excitation frequency in the 650-800 nm window, from which the excitation (action) spectra of selected processes can be recorded. The linearity of the response was checked by recording actinic power-dependence curves, obtained by attenuating the pump intensity by opal diffusers and neutral density filter combinations. The excitation wavelength was monitored by a CCD-based spectrometer (Ocean Optics). The PSI action spectra were obtained by measuring the absorption changes at 430 nm, 50 μ s after a sub-saturating flash. For the acquisition of PSI action spectra in cyanobacterial cells 20 μ M DCMU and 2 mM hydroxylamine were added to suppress PSII contributions.

Fluorescence spectroscopy

1) Time-resolved fluorescence spectroscopy at room temperature

a) Figure S1. Time-correlated single-photon counting measurements were performed using a FluoTime 200 picosecond fluorometer (PicoQuant). Fluorescence lifetime decay kinetics were measured at room temperature on intact cells with addition of 50 μ M DCMU. Excitation was provided by a 470 nm laser diode using a 10 MHz repetition rate. These settings as well as the laser intensity were chosen to be far below the onset of singlet-singlet exciton annihilation (<0.1 pJ). Fluorescence was initially detected at 680 nm with 1 nm slit-width and then recorded in the 630–770 nm detection region with 2 nm steps. The resolution of the time-to-amplitude converter was 4 ps per channel. The instrument response function was 50 ps. The results were analyzed by a global iterative re-convolution procedure, considering a linear combination of weighted exponential functions as a model decay curve (18–20) using FluoFit software (PicoQuant). The fit considers the lifetimes as global (wavelength-independent) parameters, whereas the pre-exponential parameters are not constrained. A plot of the pre-exponential amplitudes as a function of the observation (emission) wavelength yields the decay-associated spectra. The quality of the fits was judged by the χ^2 parameter.

b) Figure 2D. Changes in fluorescence yield in *C. thermalis* cells (10 μ g chlorophyll ml⁻¹) were measured using a JTS-10 spectrophotometer (Bio-Logic) as described by (12). The

fluorescence yield was probed using weak detecting flashes of 4 μs at 420 nm with negligible actinic effects. Green and far-red actinic illumination was provided by LEDs at 520 nm ($700 \mu\text{mol photons m}^{-2} \text{s}^{-1}$) and 740 nm ($1700 \mu\text{mol photons m}^{-2} \text{s}^{-1}$), respectively. The rate of Q_A reduction in PSII was estimated by measuring the kinetics of fluorescence rise in the presence of 20 μM DCMU.

c) Figure 1C. The PSII action spectra were obtained as described in above in the section 4b of the material methods and using the same instrument but measuring Q_A^- accumulation in the presence of 20 μM DCMU via the fluorescence change induced by a sub-saturating flash.

2) Fluorescence spectroscopy at low temperature

a) Figure S10. Fluorescence of isolated PSI and PSII was measured as described by (21) using a 1 mW HeNe laser (633 nm) or light from Spex 0.25 M double monochromators with a halogen lamp, providing 7 $\mu\text{W cm}^{-2}$.

b) Figure 1B. Low-temperature (80K) fluorescence spectra of *C. thermalis* cells were recorded as described previously using 430 nm as excitation wavelength (22).

3) Kinetics of Q_A^- accumulation at 293K and 77K using fluorescence

a) Figure 1D. The rate of Q_A^- formation was determined in *C. thermalis* cells ($10 \mu\text{g chlorophyll ml}^{-1}$) in the presence of 20 μM DCMU using a JTS-10 spectrophotometer (Bio-Logic) by measuring the fluorescence emission (11). Green and far-red actinic illumination was provided by LEDs at 520 nm ($700 \mu\text{mol photons m}^{-2} \text{s}^{-1}$) and 740 nm ($1700 \mu\text{mol photons m}^{-2} \text{s}^{-1}$), respectively (12). The intensity of the two actinic light was set empirically so as to obtain measureable rates of Q_A^- accumulation with both green and far-red light. The fluorescence kinetics were normalized to the F_{max} measured after a saturating pulse.

b) Figure 2B. The kinetics of Q_A^- accumulation were measured at 293K and 77K by recording the fluorescence emission at 750 nm when exciting with 600 nm and 710 nm in a PerkinElmer LS50B fluorometer. The excitation wavelengths were chosen in order to have i) an equivalent absorption cross section at each excitation wavelength based on the absorption spectrum of the thylakoid sample, and ii) an equivalent photon flux based on the spectrum of the instrument xenon lamp. A neutral density filter (0.2 from Thorlabs cutting ~60% of transmission) was used for the excitation light in order to slow-down the kinetics at room temperature. Samples, *C. thermalis* thylakoids ($5 \mu\text{g chlorophyll ml}^{-1}$ in buffer A) were pre-illuminated at room temperature for 10 seconds with room light of $50 \mu\text{mol photons m}^{-2} \text{s}^{-1}$ and then dark-adapted for 10 min. The samples were loaded in the dark. In both cases a manual shutter was opened to start the reaction.

Structural analysis

Amino acid sequences for the subunits of FRL-PSII and FRL-PSI contained in the FaRLiP (23) gene cluster from *C. thermalis* were compared with those in other FaRLiP-containing species. The FRL-sequences were also compared to those of WL-photosystems in species with and without the FaRLiP. In particular the sequences from *T. vulcanus* and *T. elongatus* were used in the sequence alignment in order to locate relevant amino acid residues based on the well-resolved crystal structures from these two species (8, 24).

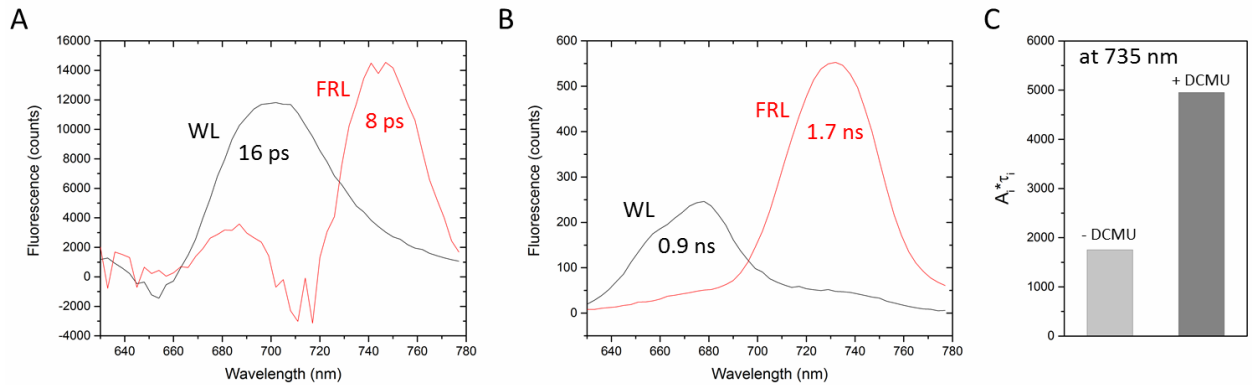
For PSII, amino acid sequences were aligned with Clustal Omega (25) including the following sequences: i) FaRLiP gene cluster sequences in *C. thermalis* (Chro_1031 PsbA; Chro_1037 PsbD; Chro_1038 PsbC; Chro_1039 PsbB; Chro_1041 PsbH) and their orthologs in the following strains: *Fischerella* sp. JSC-11, *Calothrix* sp. PCC 7507, *Pleurocapsa* sp. PCC 7327 and *Oscillatoriales cyanobacterium* sp. JSC-12; ii) sequences from the equivalent paralogs expressed in white light from *C. thermalis* (Chro_4335 PsbA; Chro_1679 PsbD; Chro_1212 PsbC; Chro_5453 PsbB; Chro_5124 PsbH); and iii) PSII sequences from *T. elongatus*, *T. vulcanus* and *Synechocystis* sp. PCC 6803.

For PSI a sequence alignment was constructed using Clustal Omega (25) with the following sequences: a) FaRLiP gene cluster sequences in *C. thermalis* (Chro_1019, PsaA; Chro_1018, PsaB) and their orthologs in the following strains, *Fischerella* sp. JSC-11, *Calothrix* sp. PCC 7507, *Pleurocapsa* sp. PCC 7327 and *Oscillatoriales cyanobacterium* sp. JSC-12; b) sequences from the equivalent paralogs expressed in white light from *C. thermalis* (Chro_5026, PsaA; Chro_5027, PsaB); and c) PSI sequences from *T. elongatus* and *Synechocystis* sp. PCC 6803.

3D-models for FRL-PSII and FRL-PSI, were built with SWISS-MODEL (26) using 4YUU (27) and 4KT0 (28) as templates for PSII and PSI respectively. The cofactors were added to the models from the crystal structure upon structural alignment. The models, together with the crystal structures (8, 24), were used to analyze the amino acid residues conserved among the FaRLiP cluster genes in the species listed above, in order to obtain insights on the location of chl*f* and chl*d* pigments in FRL-PSII and FRL-PSI. Residue numbering, when given, is according to the sequence of *C. thermalis* in the FaRLiP cluster. The equivalent numbering in *T. vulcanus* or *T. elongatus* are also given to help relate to the crystal structure.

Structure visualization and analysis was carried out with PyMOL (The PyMOL Molecular Graphics System, Version 2.0 Schrödinger, LLC).

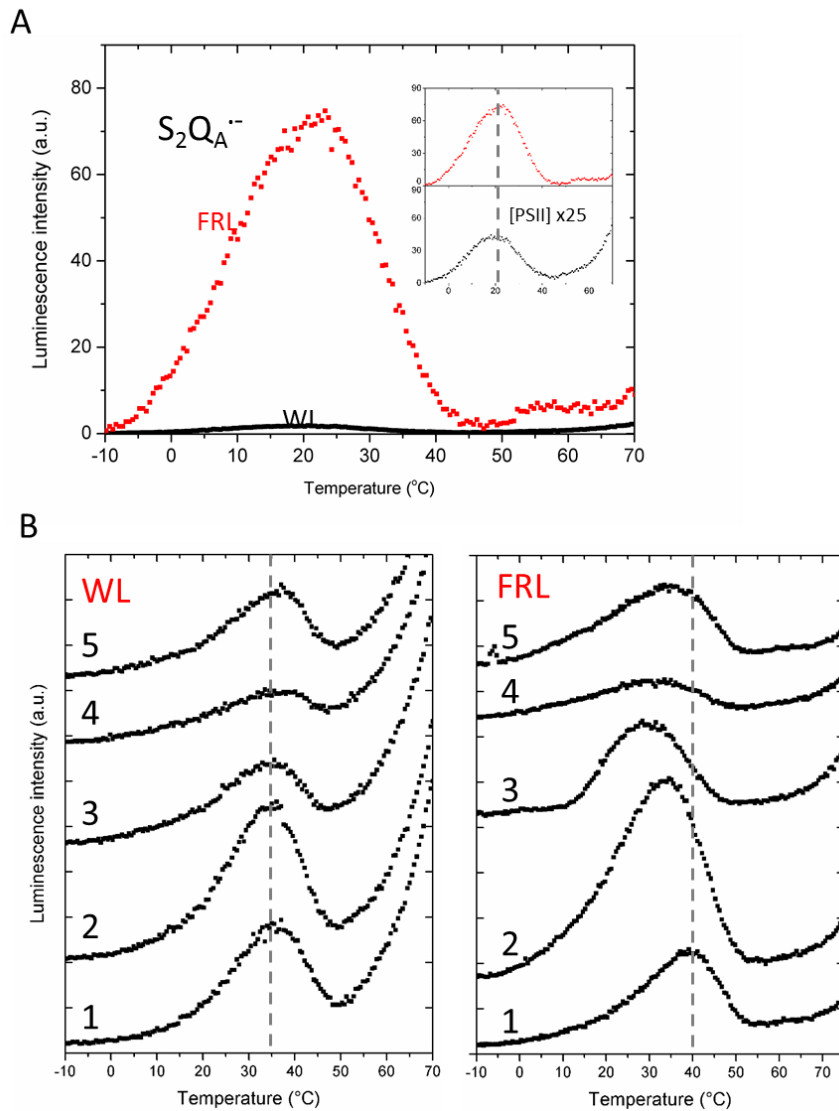
Fig. S1.



Excited state relaxation at 293K in white light (WL) and far-red light (FRL) grown *C. thermalis* cells.

(A) Representative decay associated spectra (DAS) from the fastest components obtained for WL (20 ± 7 ps) and FRL-cells (12 ± 4 ps), which are largely dominated by excited state relaxation attributed to PSI (29). A broad maximum in the 700-720 nm region in WL-cells is characteristic for chl a -PSI (30). The red-shift DAS in FRL-cells with a maximum at 750 nm is consistent with the presence of long-wavelength chlorophylls in the core of PSI. The small positive feature centered at ~690 nm, accompanied by a negative feature at 720 nm is a typical signature of excited state energy transfer from short to long-wavelength chromophores (18, 19). (B) Representative DAS associated to the longest-lived excited state relaxation components, mainly assigned to PSII (31–33). The DAS of the longest-lived component in WL-cells (0.84 ± 0.05 ns) show a maximum at ~680 nm. The pronounced shoulder at ~660 nm is associated with residual emission from phycobilisomes. In FRL-cells, the DAS of the longest-lived component (1.76 ± 0.08 ns) shows a red-shifted maximum to 735 nm, which is consistent with the presence of long wavelength chlorophylls in PSII. (C) Contribution of the longest-lived component of FRL-grown cells at 735 nm to the steady state emission in the presence of DCMU. The 2-fold increase confirms the assignment of the component to PSII under these conditions.

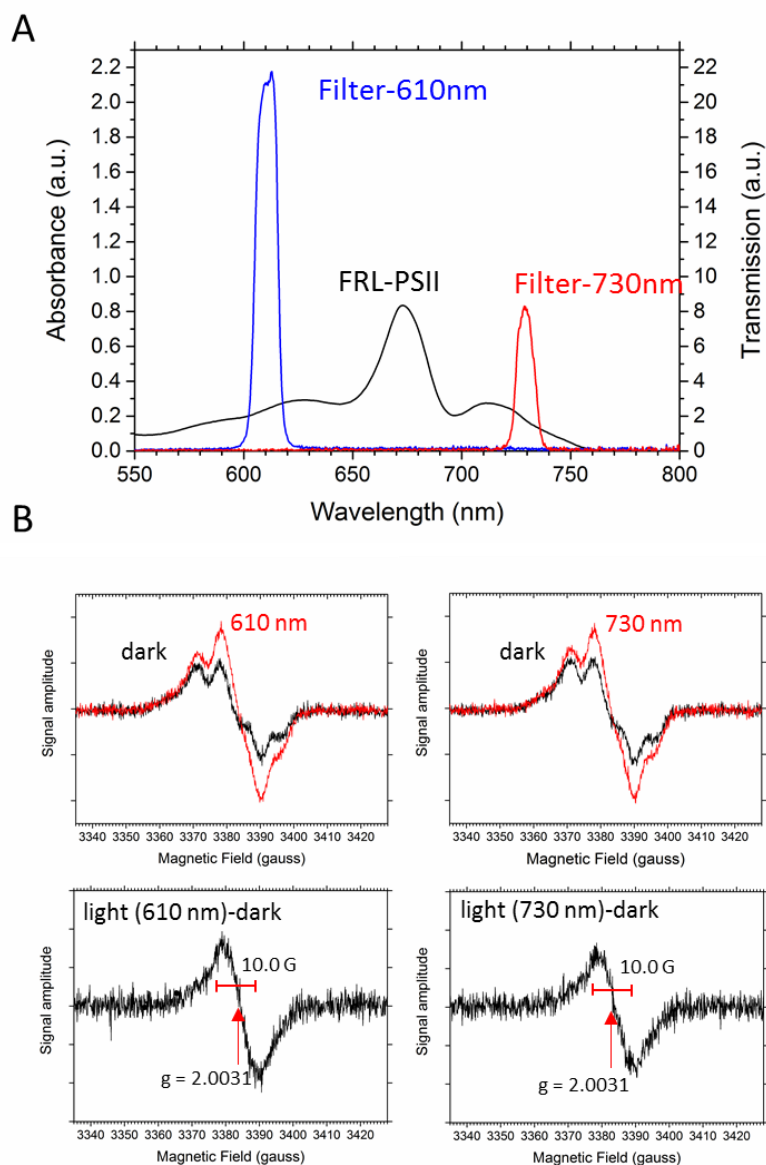
Fig. S2.



Characterisation of PSII by thermoluminescence using WL and FRL grown *C. thermalis* thylakoid membranes.

(A) The $S_2Q_A^{\cdot-}$ recombination in FRL is >25-times higher than in WL membranes when compared in terms of active PSII. The FRL sample was diluted to 25-times less PSII than in the WL sample (inset). (B) Flash dependency of luminescence intensity and peak position. A cycle of 5 flashes is shown.

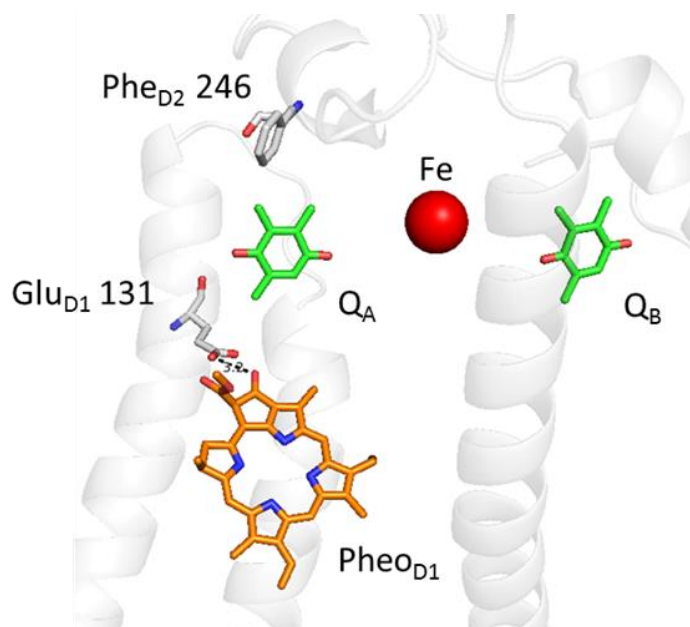
Fig. S3.



Characterization of FRL-PSII by EPR.

(A) Absorption spectrum of isolated FRL-PSII and filter transmission profiles. Filters were chosen at regions of similar absorbance (610 nm and 730 nm). (B) Tyr_D radical in FRL-PSII illuminated with 610 nm (red, top, left) and 730 nm (red, top, right) in comparison to their dark spectrum (black). The corresponding light-dark difference spectra are shown in the bottom panel. A g -value of 2.0031 and a peak width of 10.0 G were determined for the light induced radical attributed to Car⁺. The stable Tyr_D[•] radical was present in the dark. EPR conditions: microwave power, 5 μ W; modulation amplitude, 2.8 G; conversion time (= time of integration/pt), 20 ms; 16 accumulations, temperature, 15K.

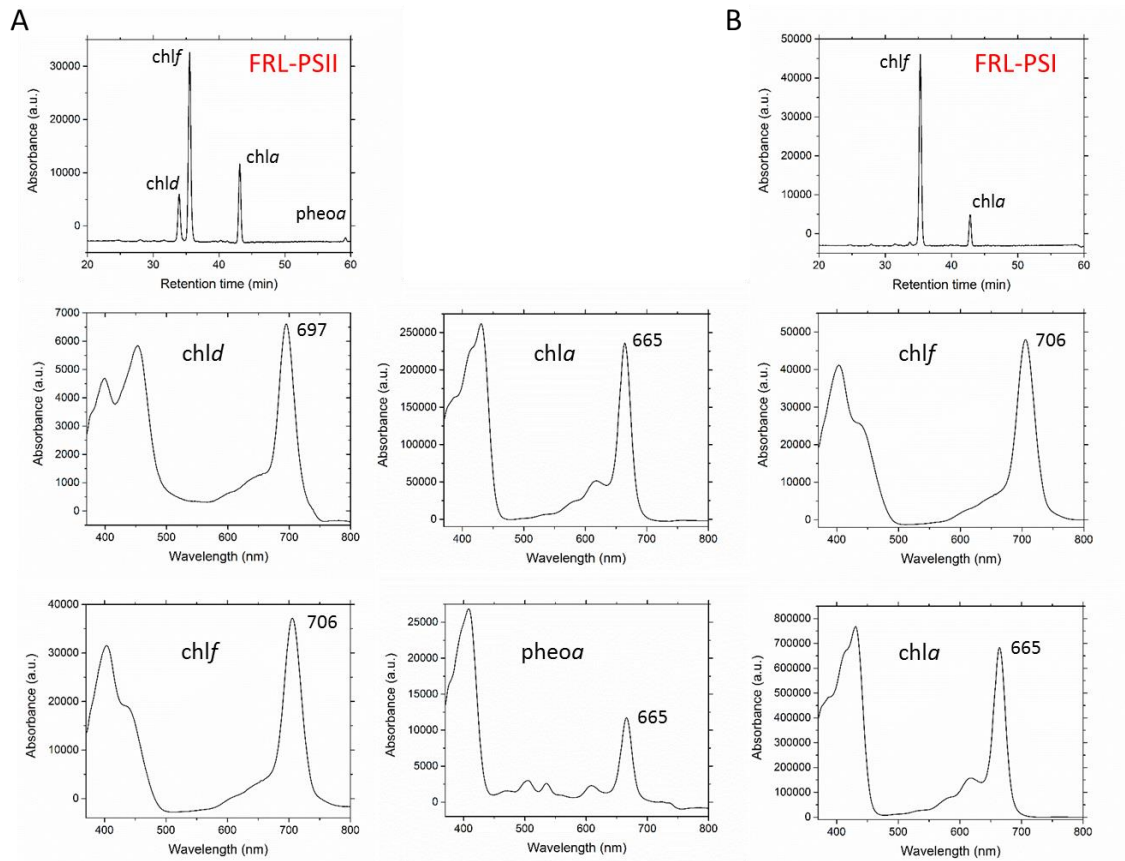
Fig. S4.



Conserved amino acid changes related to redox-tuning of Phe_{OD1} and Q_A.

Glu_{D1} 131 (Gln_{D1} 130 in *T. elongatus*) is well conserved in FRL-PSII. This residue is found in PsbA in chloroplasts and cyanobacterial isoforms associated with acclimation response to growth in high light. Substitution of Gln_{D1} 130 with Glu_{D1} in *T. elongatus* has been shown to increase the strength of the H-bond with Phe_{OD1} resulting in a shift of the Pheo reduction potential to more positive values (34). Q_x absorption region shows an electrochromic blue-shift of Phe_{OD1} upon reduction of Q_A⁻ (35), known as the C-550 band-shift (centered at around 545 nm). The stronger H-bond from the carboxylic group of Glu_{D1} 130 to the 13-keto group of Phe_{OD1} results in a 3.0 nm red-shift of the C-550 band-shift (36). A conserved change in FRL-PSII in proximity of Q_A, Phe_{D2} 246 (Met_{D2} 246 in WL-PSII and *T. elongatus*), could be involved in redox tuning of the primary quinone.

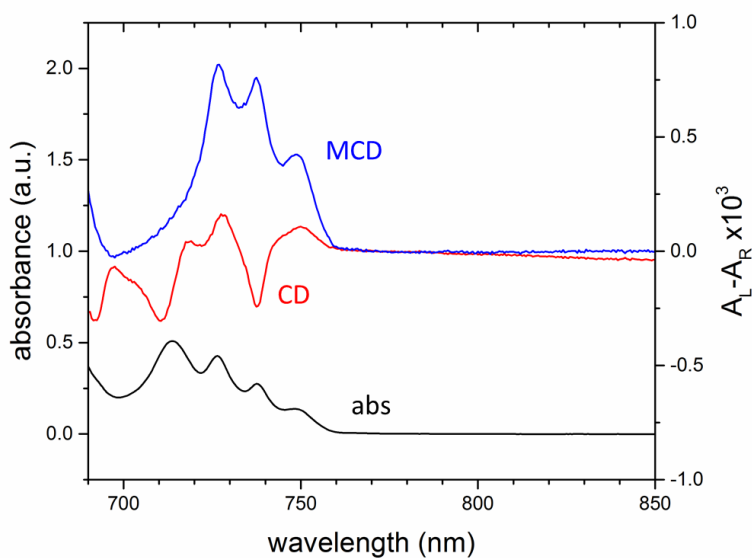
Fig. S5.



Pigment composition analysis of purified FRL-photosystems by HPLC.

(A) FRL-PSII (B) FRL-PSI. Partial PDA chromatograms at 707 nm (top row) show peaks of pigments that were assigned by their corresponding absorption spectra as shown in the panels below. In PSI *chl_f* (retention time 35.29 min) and *chl_a* (42.82 min) were identified. In PSII *chld* (33.80 min), *chl_f* (35.45 min), *chl_a* (42.98 min) and *pheo_a* (59.13 min) were identified.

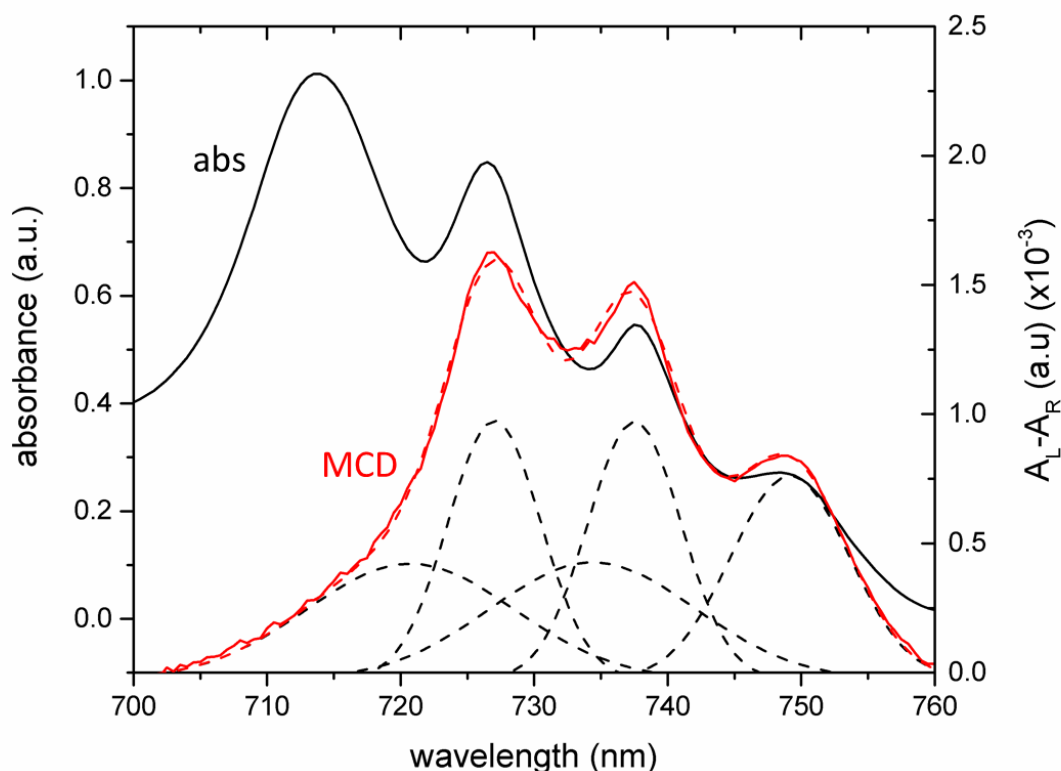
Fig. S6.



Low-temperature (1.8K) absorption (black), MCD (blue) and CD (red) spectra of isolated FRL-PSII.

The low temperature absorption spectrum shows four peaks in the long-wavelength region at 712 nm, 727 nm, 737 nm and 748 nm. The 714 nm peak is strongly reduced in the MCD spectrum confirming the assignment of the peak to long-wavelength allophycocyanin. In the CD spectrum the excitonic at (-) 712 nm and (+) 719 nm and also at 794 nm are attributed allophycocyanin. Note that unlike the sample used in Fig. 2, this sample had not undergone the ion exchange chromatography step and so showed more contamination from allophycocyanin.

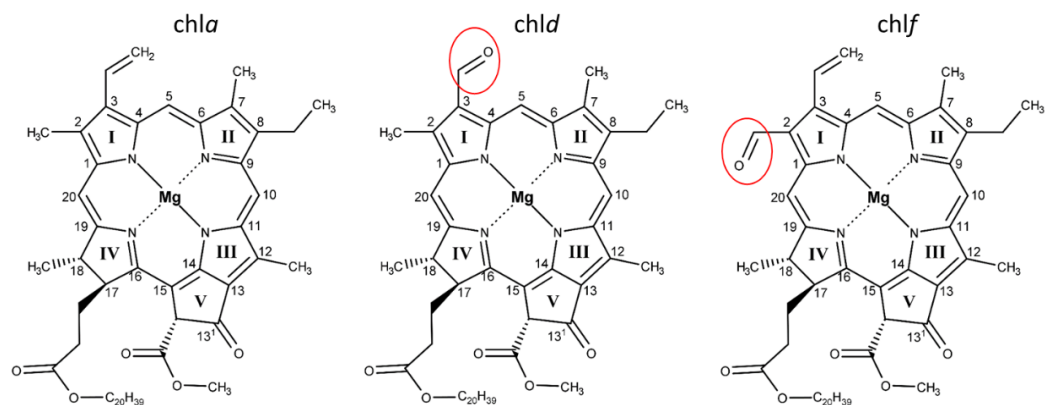
Fig. S7.



Low temperature (1.8K) MCD (red) and absorption spectrum (black) of isolated PSII plus curve fitting.

The MCD and absorption spectra were obtained at 1.8K using isolated PSII as described in the materials and methods. Note that the contaminant allophycocyanin with an absorption peak at 712 nm does not show a MCD peak. Thus the MCD spectrum was used for the fitting of the five chlorophylls. OriginPro 2015 software was used. The fitting took into account the different intensities of some peaks in the MCD vs the absorption. The following results were obtained: FRL-chlorophylls were present at 721, 727, 734, 737 and 749 nm with approximately equal concentrations. The fitted Gaussians are shown in dashed black lines, the cumulative fit is shown in a red dashed line and matches the MCD spectrum.

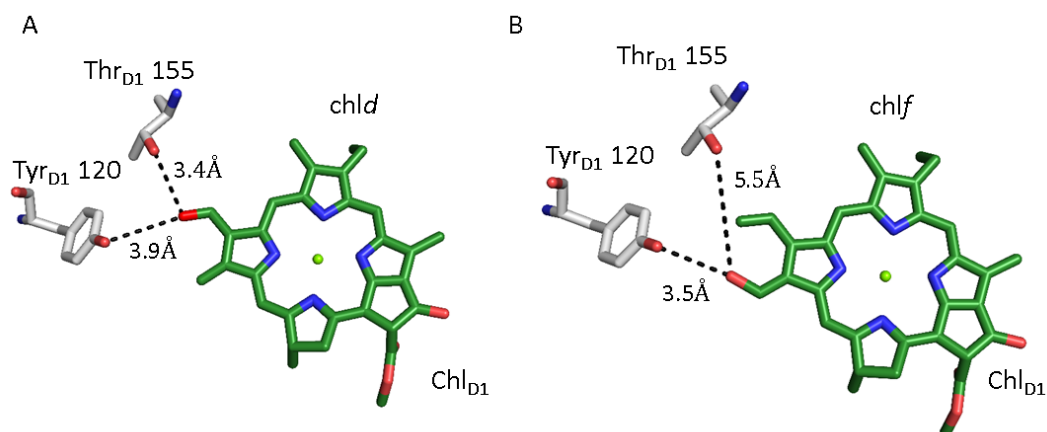
Fig. S8.



Structure of chlorophylls *a*, *d* and *f*.

Chl f and *chld* differ from *chl a* in that they both have an additional formyl substitution in ring I. The methyl group in position C2 of *chl a* is a formyl group in *chl f*, while the vinyl group in position C3 in *chl a* is a formyl group in *chld*. The replacement of the methyl group by the bigger formyl group in *chl f* is more sterically significant than replacing the vinyl group with the structurally similar formyl group in *chld*. The formyl group in *chl f* and *chld* makes them more hydrophilic than *chl a*. When incorporated into the photosystems, however, stabilization by H-bonding could occur but is likely to be uncommon as it would modify the redox and absorption properties of the chlorophyll. The electron withdrawing properties of the formyl group in either position C7 (in *chl b*) or C2, (in *chl f*), increases the Lewis acidity of the Mg^{2+} atom compared to *chl a*. In contrast in *chld*, where the electron withdrawing vinyl group in position C3 is substituted with a formyl group, the Lewis acidity of the Mg^{2+} remains similar to that in *chl a* (37, 38). The increase in Lewis acid strength in *chl f* (and also *chl b*) is predicted to disfavor the displacement of the Mg^{2+} -bound water by a protein ligand. This would decrease the affinity of the chlorophyll for the protein binding site (37, 38). Histidine, the most common chlorophyll ligand, is thus considered a relatively poor ligand for *chl f*, with other ligands containing oxygen (e.g. carboxylic acids, alcohols and water) being better candidates (see fig.S11 and fig. S19).

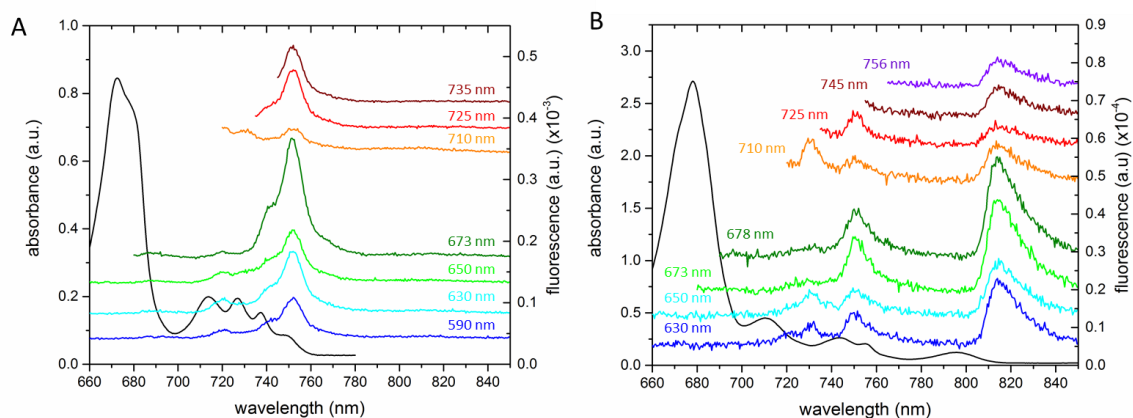
Fig. S9.



Modelling of potential H-bonds to FRL-Chl_{D1} in FRL-PSII.

Potential H-bonds from Tyr_{D1} 120 and Thr_{D1} 155 to the formyl group located in either position C3 (A) as in *chl_d* or in position C2 (B) as in *chl_f*. These H-bonds could stabilize these more hydrophilic chlorophylls in this location and destabilize *chl_a*. The H-bond would also increase the redox potential, which could be important for redox tuning. By compensating some of the negative charge on ring I, which is on the Q_y axis dipole, the H-bond would blue-shift the absorption relative to the non-H-bonded chlorophylls, consistent with an absorption at 727 nm, one of the shorter wavelength chlorophylls of the FRL-chlorophylls in FRL-PSII. The equivalent of the Tyr_{D1} 120 and Thr_{D1} 155 in *C. thermalis* are also conserved in *Acaryochloris* sp., where *chl_d* occupies the Chl_{D1} position and gives an electrochromic band shift at 723 nm (39–41), very similar to the situation reported here (Fig. 2). These observations support the already strong assignment of the Chl_{D1} being replaced by either *chl_f* or *chl_d* but do not favor one over the other.

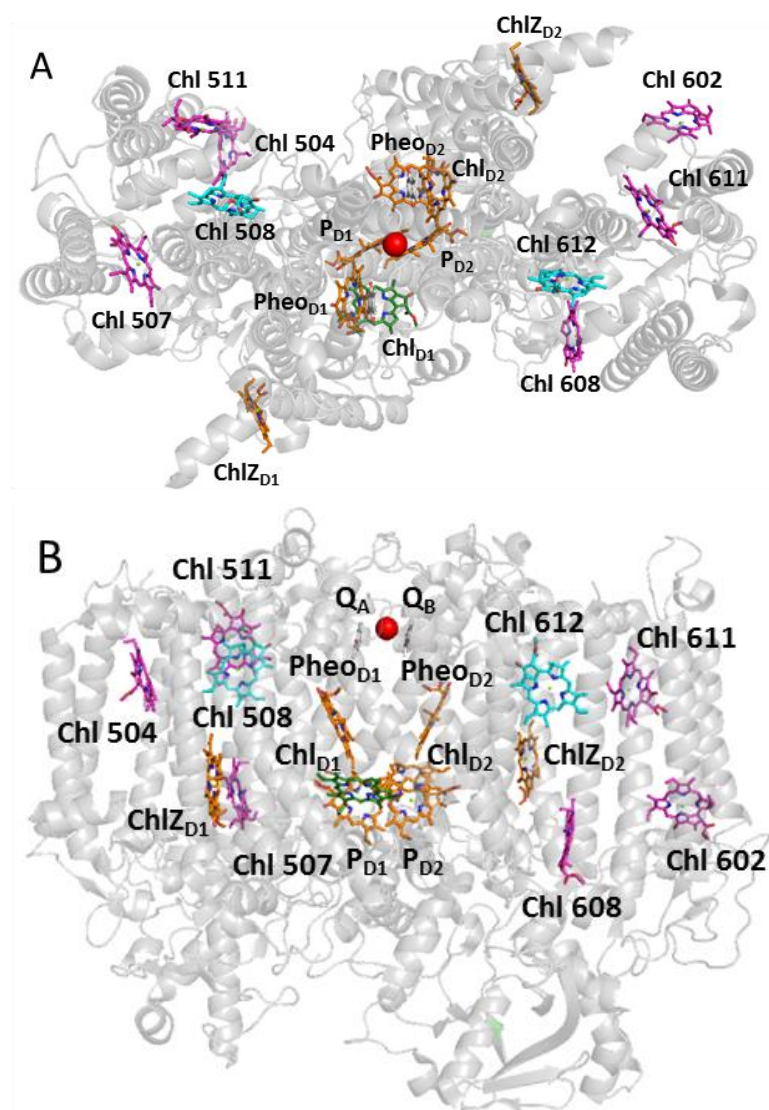
Fig. S10.



Excitation dependence of fluorescence emission at 1.8K in isolated FRL-PSII (A) and FRL-PSI (B).

Fluorescence spectra were collected at a series of wavelengths from 590 nm to 756 nm using matched excitation intensities. The black spectra are the absorption spectra at 77K of the test sample. Note this preparation had a marked contamination from long-wavelength allophycocyanin (absorption peak at 712 nm) as it had not undergone the anion exchange chromatography step used in most of the other experiments. For PSII the maximum emission is at 755 nm at all excitation wavelengths. The 755 nm emission is lowest when exciting at 710 nm, suggesting that the allophycocyanin (712 nm) is poorly connected to PSII in terms of exciton transfer. The emission peak at 720 nm could be from allophycocyanin but there is also a shoulder at 740 nm which has previously been attributed to the emission from this pigment (42). The 755 nm emission is bigger when excited at 673 nm, the peak of *chl a* absorption, and there is very little *chl a* fluorescence (685-700 nm), indicating that essentially all the *chl a* is connected directly or indirectly to *chl f*. The fluorescence below 650 nm is emitted from a contaminant of disconnected shorter wavelength phycobilisomes. PSI shows a maximum emission at 812 nm at all excitation wavelengths. Two additional peaks at 730 nm and 755 nm are visible. The 730 nm emission is biggest when excited at 710 nm suggesting that the allophycocyanin is poorly connected to PSI. The emission wavelength fits well with previous observations made for isolated allophycocyanin in other species (43, 44). The emission at 755 nm indicates a minor contamination of the sample with PSII while no PSI contamination in PSII was seen.

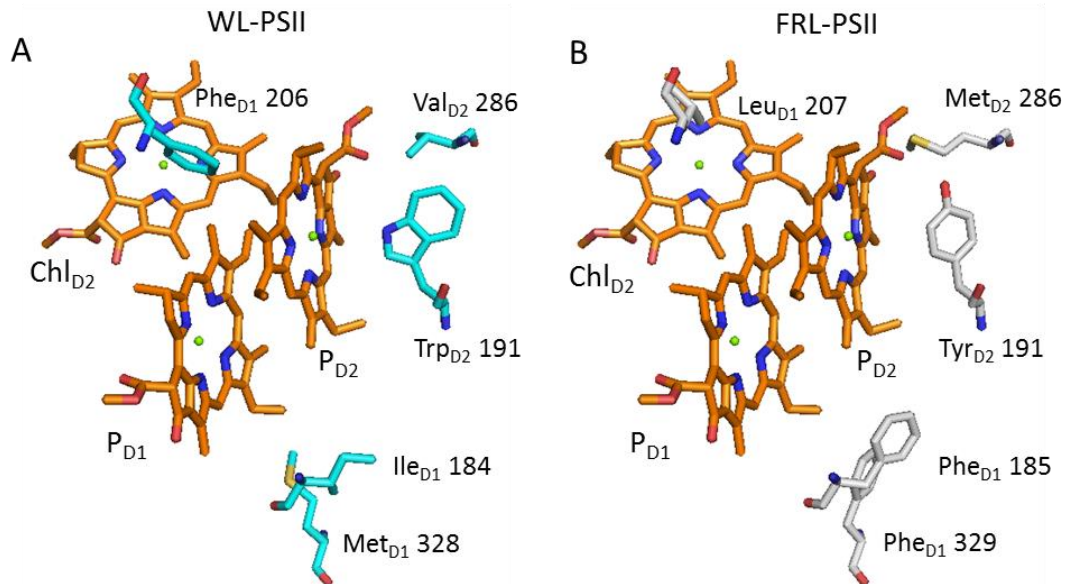
Fig. S11.



Chlorophylls ligated by ligands other than His in PSII CP43 and CP47.

Non-His ligated chlorophylls from PSII (PDB: 3WU2) are shown in pink. D1, D2, CP43 and CP47 are shown as cartoon in light grey. The structure is shown in two orientations (A) top view and (B) side view. Chl 508 (CP43) and Chl 612 (CP47), both coordinated by His, are shown in cyan as they are the closest chlorophylls in the antenna to Chl_{D1}, which is shown in green. All the other reaction centre (D1 and D2) chlorophylls are shown in orange. The quinone rings (silver) and the non-heme iron (red sphere) are also shown. The chlorophyll phytyl tails have been removed. The non-histidine chlorophyll ligands are as follows: i) CP43: Chl 504 (lipid DGDG5); Chl 507 (Ser C275); Chl 511 (Asn C39); ii) CP47: Chl 602 (Trp B185); Chl 608 (lipid DGDG14); Chl 611 (H₂O). Chl*f* is expected to prefer non-His ligands (see fig. S8).

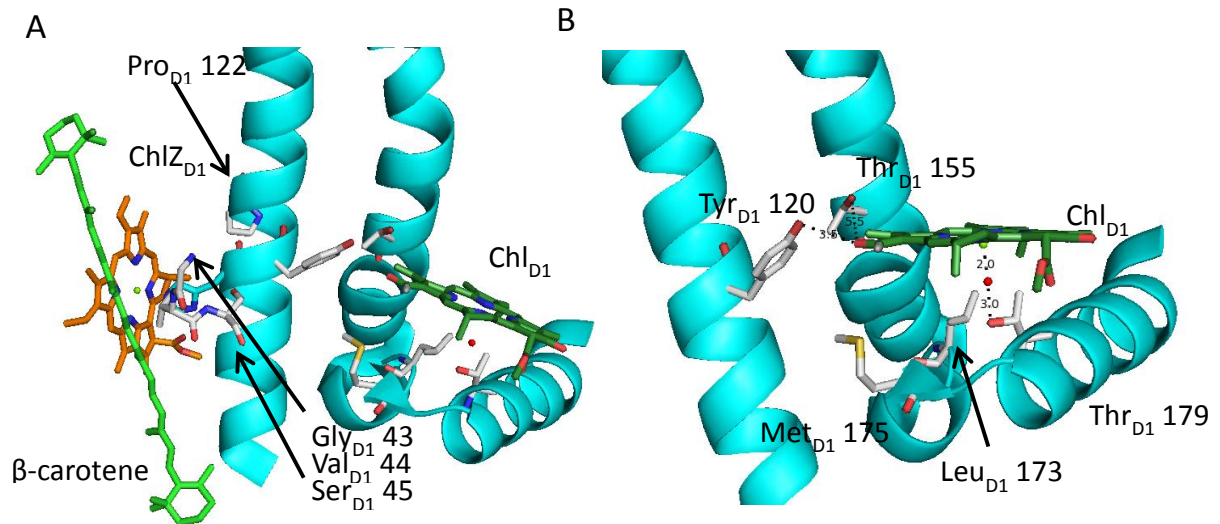
Fig. S12.



Conserved amino acid changes around Chl_{D2}, P_{D1} and P_{D2} in FRL-PSII.

A conserved residue Leu_{D1} 207, which is a Phe_{D1} in normal WL-PSII (Phe_{D1} 206 in *T. elongatus*), is located close Chl_{D2} in FRL-PSII. Phe_{D1} 206 is 3.7 Å from the C10 of Chl_{D2} between ring II and III and perpendicularly oriented with respect to the chlorophyll ring. It is also within 4 Å from P_{D1} and P_{D2}. The loss of this aromatic ring in FRL-PSII will likely affect these pigments and, in particular, as it is 3.7 Å from the positive pole of the transition dipole ($\vec{\mu}$) of Chl_{D2}, its substitution with Leu could result in a blue-shift of the chlorophyll absorption spectrum. The effect on P_{D1} and P_{D2} could be compensated by another conserved change within 4 Å from both chlorophylls, Phe_{D1} 185, which is Ile_{D1} 184 in WL-PSII in *T. elongatus*. A second aromatic residue change occurs close to Phe_{D1} 185, Phe_{D1} 329 (Met_{D1} 328 in WL PSII and *T. elongatus*) increasing the effect of aromatic π -stacking. These changes could be related to the substitution of *chl a* by a long wavelength chl in the Chl_{D2} position but they could also be there to retune a *chl a* Chl_{D2} in the presence of the long wavelength chlorophyll in the Chl_{D1} position. Thus these changes do not provide clear evidence for or against the presence of a long wavelength chlorophyll at the Chl_{D2} position. Other relevant conserved amino acid changes around P_{D2}, include i) Tyr_{D1} 191 (Trp_{D2} 191 in WL-PSII) which is at van de Waals distance and perpendicular to ring III, and ii) Met_{D2} 286 (Val_{D2} 286 in WL-PSII), which is within H-bonding distance of the tyrosine. These amino acid changes seem likely to be involved in redox tuning of P_{D2} and may affect the coupling between P_{D1} and P_{D2}. This could reflect tuning of the chlorophylls to optimize the location of the cation radical on P_{D1} for efficient TyrZ oxidation.

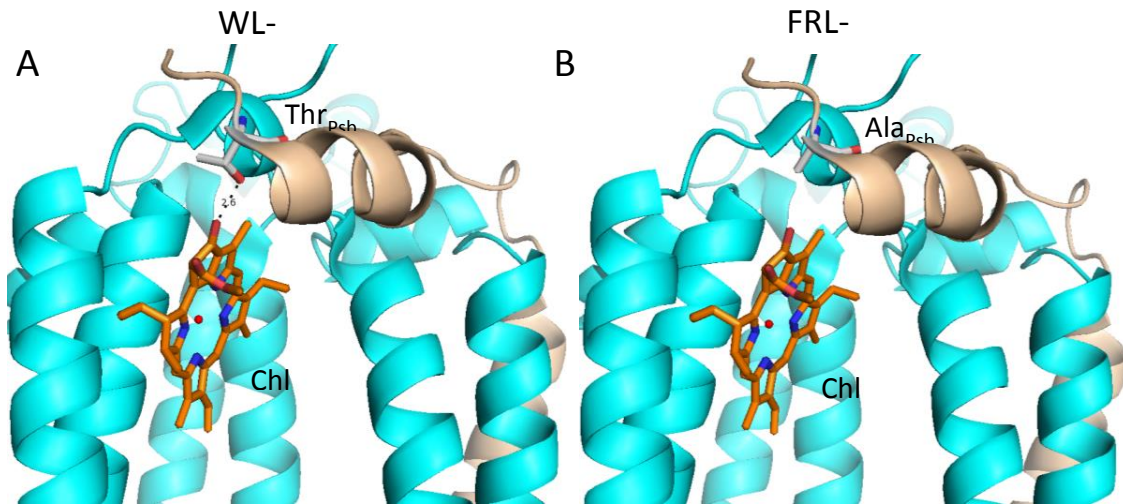
Fig. S13.



Conserved structural difference in the FRL-PSII compared to WL PSII based on sequence comparisons.

(A) A number of these differences are located between Chl_{D1} and ChlZ_{D1}. Gly_{D1} 43, Val_{D1} 44 and Ser_{D1}45 (Leu_{D1} 42, Ala_{D1} 43 and Ala_{D1} 44 in WL PSII and *T. elongatus*) might affect the position of the carotenoid close to ChlZ_{D1}. A conserved change, Pro_{D1} 122 (Ile_{D1} 121 in WL PSII and *T. elongatus*), is located in the middle of helix B and will probably introduce a kink with consequent movement of either the luminal or stromal part of the helix. (B) Conserved differences around Chl_{D1} include: Tyr_{D1} 120 and Thr_{D1} 155 (Phe_{D1} 119 and Ala_{D1} 154 in WL PSII and *T. elongatus* respectively), which are within 5 Å of the C2 position and within 4Å of the C3 position of ring I of Chl_{D1}; Met_{D1} 175 (Leu_{D1} 174 in WL PSII and *T. elongatus*) is below ring I of Chl_{D1} and could participate in the H-bonding network with Tyr_{D1} 120 and Thr_{D1} 155; Leu_{D1} 173 (Met_{D1} 172 in WL PSII and *T. elongatus*) is close to the conserved Thr_{D1} 179 that H-bonds the water molecule coordinating the Mg in Chl_{D1}. The Met_{D1} 172 in WL PSII and *T. elongatus* is probably involved in the H-bonding network to the water ligand to the Mg of Chl_{D1}. Changing this residue to Leu in FRL-PSII might disrupt this network with potential consequences on the chlorophyll binding in this position. Note that Leu_{D1} 173 is specific to the D1 proteins found in the FarLiP cluster and also that *Acaryochloris* sp., which has chl_d as Chl_{D1}, still has Met_{D1} 172 and Leu_{D1} 174 just like *C. thermalis* WL PSII.

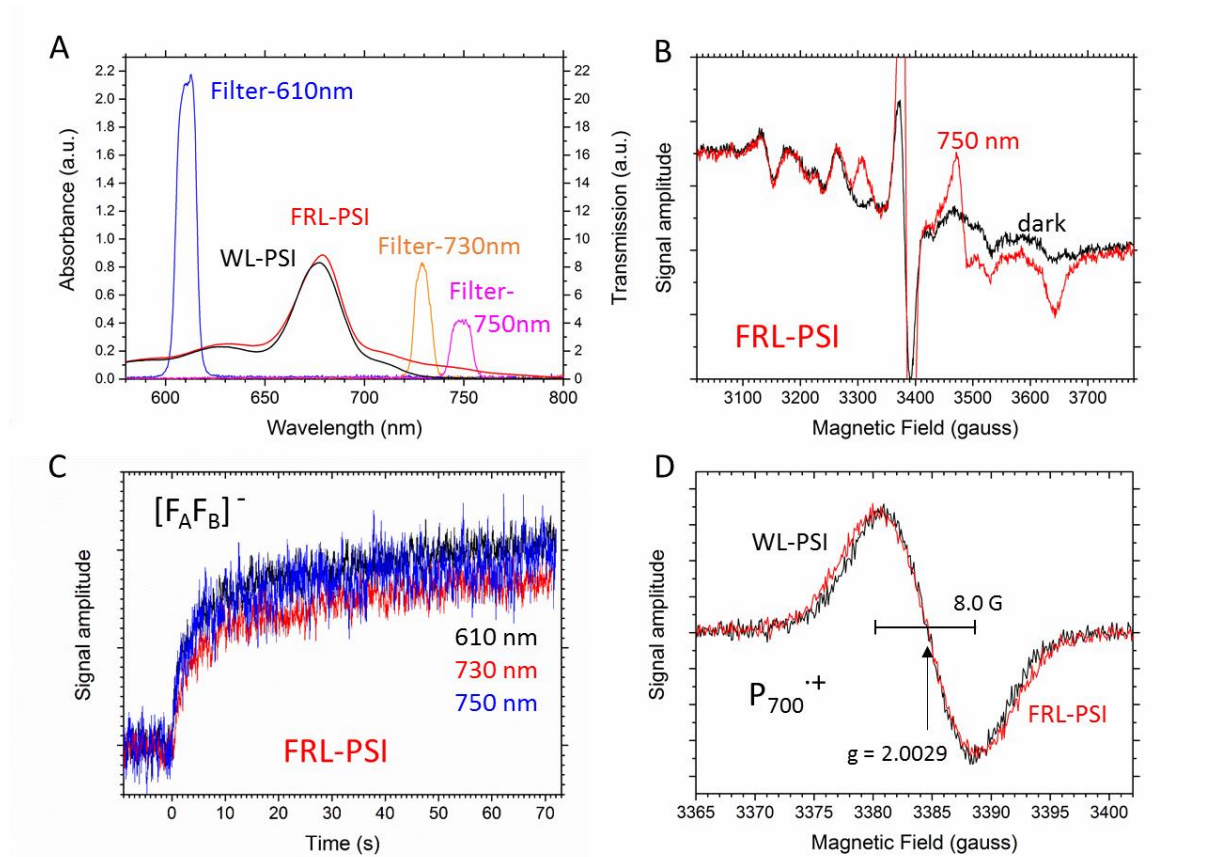
Fig. S14.



Analysis of the other PSII genes (PsbB (CP47), PsbC (CP43) and PsbH) in the FarLiP cluster.

Several conserved changes suggest re-tuning of the color of the chlorophylls, which are mainly *chl_a*, to adjust for the presence of a small number of FRL-*chl* molecules in antenna and redox roles. For example, (A) Thr5 in PsbH, has been shown to H-bond the 13-keto group of CP47 Chl617 (Chl29). This chlorophyll has been suggested to be the red-shifted trap in CP47, which is responsible for the 695 nm fluorescence band, though its assignment is still under debate (45). (B) The FRL-PsbH has a conserved change to Ala5. This will eliminate the H-bond and consequently will blue-shift Chl617 making it less likely to act as an emitter. Other examples are represented by a number of aliphatic residues substituted by Phe, placing the aromatic ring within 3 Å from a chlorophyll ring, likely resulting in either strengthening or weakening of the transition dipole depending on its location and geometry and consequently shifting the absorption spectra for that specific chromophore. Re-tuning of the *chl_a* is predicted to fit with the presence of the 5 long wavelength chlorophylls in PSII. With the only definite assignment of a long wavelength as Chl_{D1} as the primary donor, it remains likely that some of remaining 4 FRL-*chl* are present in CP43 and CP47. Thus redox tuning in these subunits will be required to optimize function. It seems clear that the well-known red shifted chlorophylls in CP43 and CP47 will no longer play that role, indeed no 685 nor 695 fluorescence was observed in FRL-PSII. It may be that color tuning has occurred to improve Forster overlap to optimize excitation from the bulk *chl_a* antenna to the far red chlorophylls perhaps with the shortest far red chlorophyll acting as a specific linker.

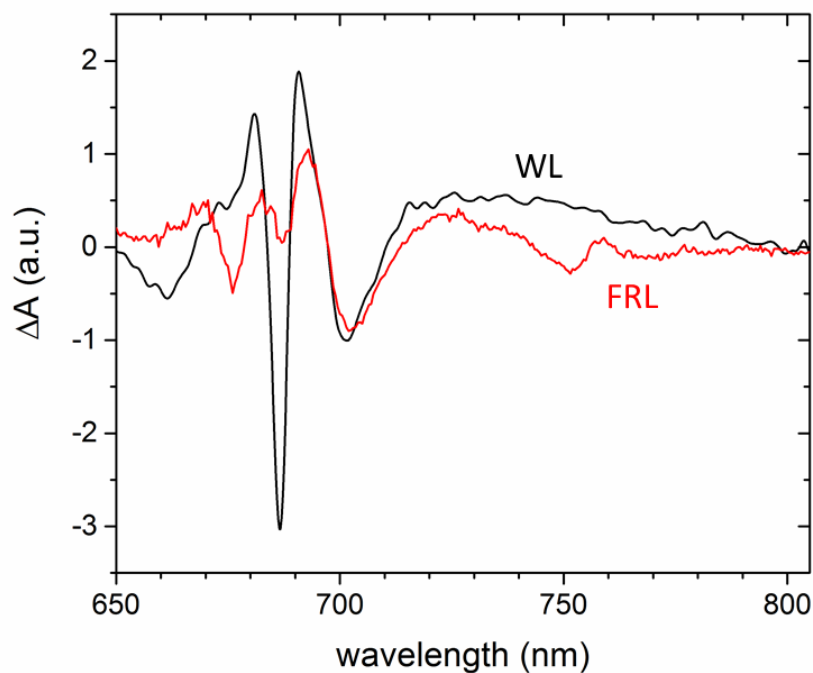
Fig. S15.



Low temperature photochemistry and EPR in isolated FRL-PSI.

(A) Absorption spectrum of isolated WL and FRL-PSI and filter transmission profiles. Filters were chosen at regions of similar absorbance (610 nm, 730 nm and 750 nm). (B) EPR spectra showing F_A reduction in FRL-PSI after illumination with 750 nm in comparison to the dark spectrum (note the dark spectrum shows the well-known "hexaquo" MnII contaminant, which is unaffected by illumination). (C) Kinetics of $[F_A F_B]^-$ formation in FRL-PSI are similar when illuminated with 610, 730 and 750 nm and match the observations of P_{700}^{+} formation in Figure 3. (D) P_{700}^{+} spectra for WL- and FRL-PSI are typical for this state, showing similar g-values (2.0029) but with slightly wider line-width in the FRL-PSII, possibly reflecting greater asymmetry in the sharing of the radical over the P_A and P_B . EPR conditions: (B) microwave power, 50 μ W; modulation amplitude, 25 G; conversion time (= time/pt), 80 ms; temperature, 15K. (C) static field, 3474 G, microwave power, 20 mW; modulation amplitude, 25 G; conversion time (= time/pt), 80 ms; temperature, 15K. A mathematical RC filter equal to 100 ms was applied after the recording of the data. (D) microwave power, 20 μ W; modulation amplitude, 2.8 G; conversion time (= time/pt), 10 ms; temperature, 15K.

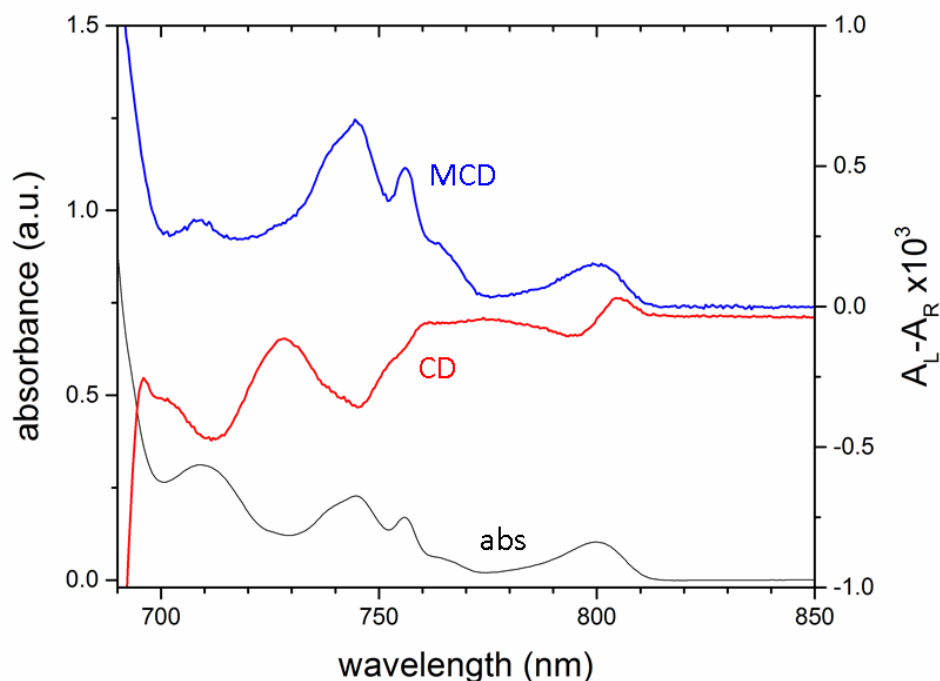
Fig. S16.



Low-temperature (77K) P_{700}^{+} difference spectrum using isolated FRL-PSI (red) and WL-PSI (black).

The 77K difference spectra were obtained as described in the materials and methods. Bleaches at 704 nm from P_{700}^{+} are present in both types of PSI but the main band-shifts in the region 675-690 nm in WL-PSI are absent in the FRL-PSI and are replaced by band-shifts at ~745 and 754 nm. The band-shifts in the FRL are better resolved in Figure 3B at higher gain and at 1.8K.

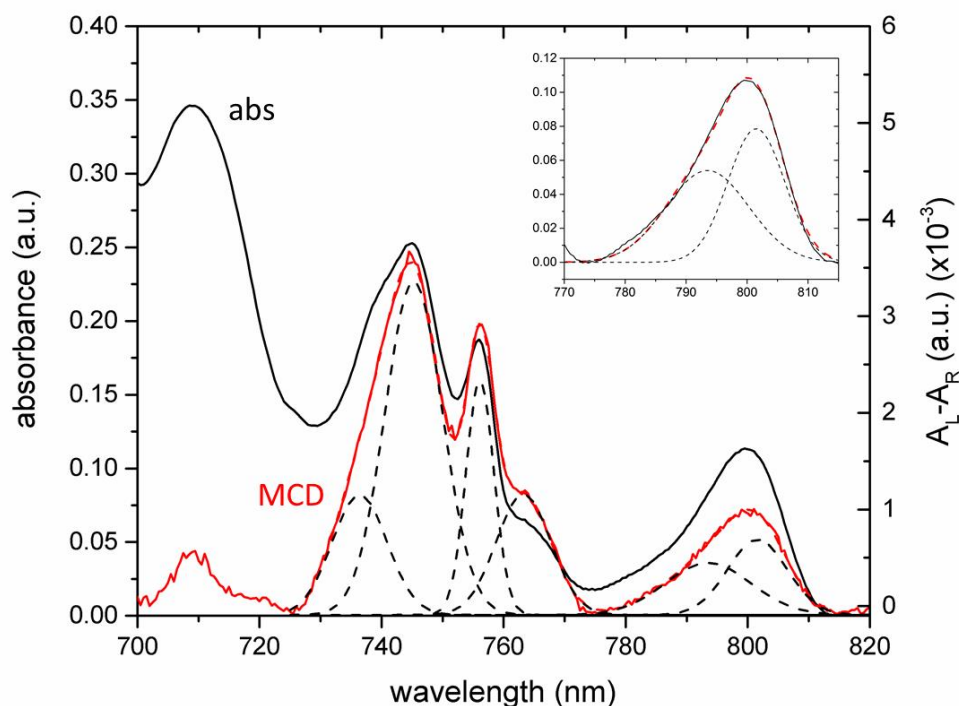
Fig. S17.



Low-temperature (1.8K) absorption (black), MCD (blue) and CD (red) spectra of isolated FRL-PSI.

The spectra were obtained at 1.8K using isolated PSII as described in the materials and methods. The low temperature absorption spectrum shows peaks in the long-wavelength region at 712, 745, 756, 764 and 800 nm. The 712 nm peak is essentially absent in the MCD spectrum confirming the assignment of the peak to long-wavelength allophycocyanin. The absence of the allophycocyanin in the MCD reveals a weak narrow peak at ~709 nm which is attributed to a long-wavelength *chl**a*. The strong peak at 745 nm with a shoulder at 736 nm corresponds to several *chl**f* molecules in a range of excitonically-coupled environments and includes some contamination from PSII in this particular preparation. The sharp peak at 756 and weak/broad peak 764 nm are each attributed to a *chl**f* molecule with weak excitonic coupling as indicated by their strong CD and weaker MCD indicating. The broad peak at ~800 nm is attributed to two strongly coupled *chl**f* molecules giving typical CD of opposite sign and weaker MCD.

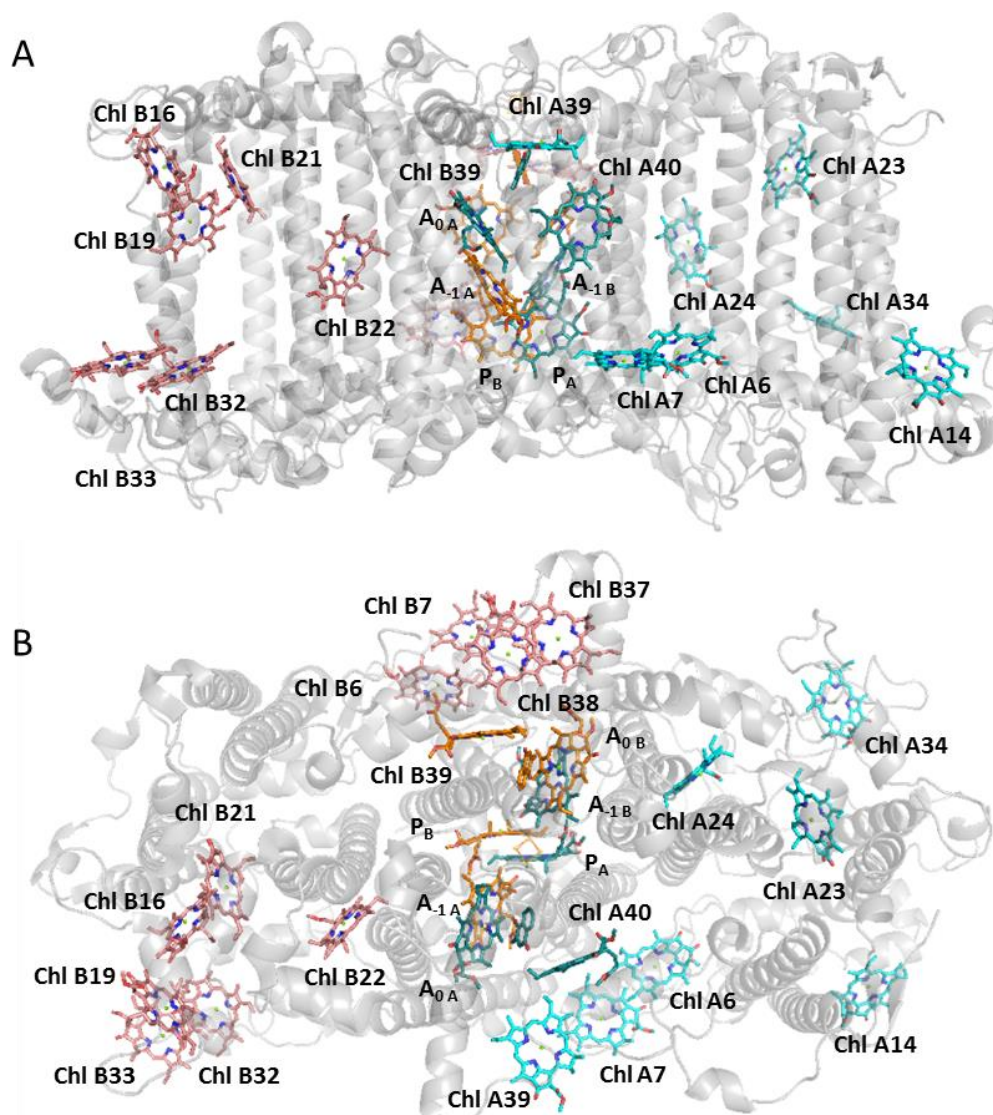
Fig. S18.



Low temperature (1.8K) MCD and absorption spectra of isolated PSI plus curve fitting.

The MCD (red) and absorption spectra (black) were obtained at 1.8K using isolated PSI as described in the materials and methods. As the allophycocyanin (~712 nm) shows little or no MCD, this spectrum was thus used for fitting. To account for the small contamination of PSII in this particular sample, a weighted fraction of the pure PSII MCD spectrum (fig. S7) was subtracted to obtain the final the spectrum for the fit, which was done with OriginPro 2015 software. The following results were obtained: FRL-chlorophylls at 736, 745 (3x), 756, 763, 794 and 802 nm were present in near equal amounts. Note that the MCD spectrum matches the absorption spectrum quite well up to 770 nm but not at longer wavelengths. The weaker MCD signal at around 800 nm (relative to the shorter wavelength peaks) leads to an underestimation of the chlorophylls in the fit of the MCD at ~800 nm. When the absorption spectrum above 770 nm was used for the fitting the area of the fitted peaks then corresponds to close to one chlorophyll under each Gaussian. The fitted Gaussians are shown in dashed black lines; the cumulative fits are shown in a dashed red line.

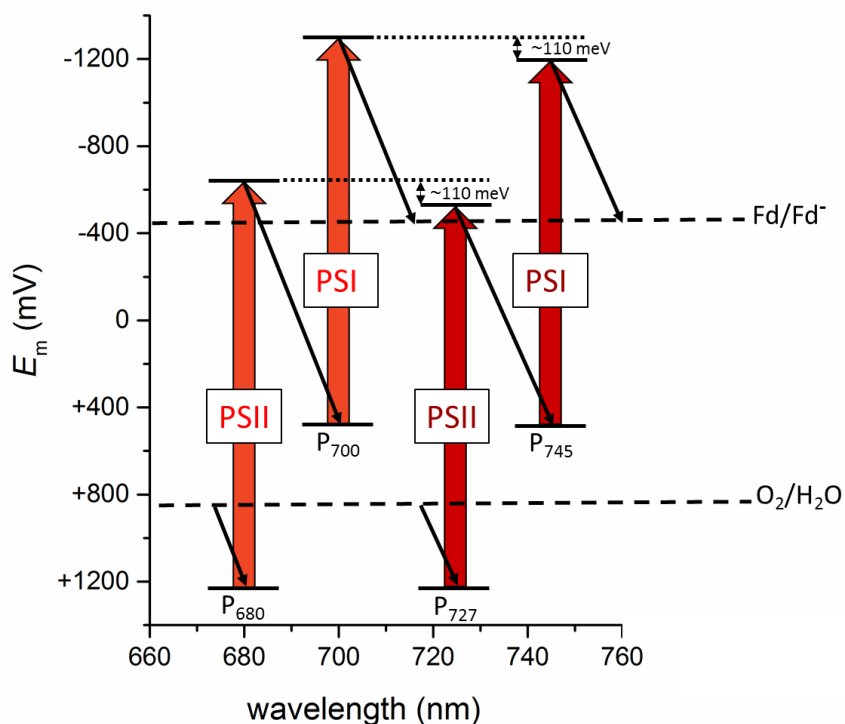
Fig. S19.



Antenna chlorophylls with ligands other than His in FRL-PSI.

These chlorophylls in PsaA and PsaB, based on the crystal structure PDB: 1JB0, are shown in cyan, for PsaA, and pink, for PsaB. PsaA and PsaB are shown as cartoon in light grey. The structure is shown in two orientations (A) side view and (B) top view. Redox active chlorophylls, phyloquinones and F_x are shown in blue (PsaA) and orange (PsaB). The chlorophyll phytol tails have been removed. The non-His chlorophyll ligands are as follows: i) PsaA: Chl A6 (Gln A115); Chl A7 (Gln A123); Chl A14 (H₂O); Chl A23 (H₂O); Chl A24 (H₂O); Chl A34 (Thr A501); Chl A39 (H₂O). ii) PsaB: Chl B6 (Asp B92); Chl B7 (Gln B94); Chl B16 (H₂O); Chl B19 (H₂O); Chl B21 (Tyr B329); Chl B22 (H₂O); Chl B32 (H₂O); Chl B33 (H₂O); Chl B37 (H₂O); Chl B38 (H₂O).

Fig. S20.



Schematic comparison of photosynthetic electron transport in WL- (red) and FRL- (dark red) photosystems based on their estimated redox potentials (E_m).

We assume that the redox potential of the oxidizing species remains the same in the FRL-photosystems and the energy shortfall is incorporated in the electron acceptor side reactions based on the situation in *Acaryochloris marina* (46, 47). The thick red arrows indicate the energy of the first excited singlet state of the primary donor, which corresponds to the energy available for charge separation. The black arrows show the electron transfer and redox changes associated with achieving the chemical activities of the photosystems and the other photosynthetic electron transfer steps, some of which are linked to PMF generation. The primary electron donors in WL-PSII (P_{680}) and WL-PSI (P_{700}) are shifted by ~ 45 nm in FRL-PSII (P_{726}) and FRL-PSI (P_{745}) but the ~ 20 nm difference between PSI and PSII is maintained. E_m values for WL-PSII and WL-PSI were used from (48) and (49) respectively.

References

1. R. W. Castenholz, Culturing Methods for Cyanobacteria. *Methods Enzym.* **167**, 68–93 (1988).
2. Y. Li, Y. Lin, P. C. Loughlin, M. Chen, Optimization and effects of different culture conditions on growth of *Halomicronema hongdechloris* – a filamentous cyanobacterium containing chlorophyll f. *Front Plant Sci.* **5**, 1–12 (2014).
3. B. Hankamer *et al.*, Isolation and biochemical characterisation of monomeric and dimeric photosystem II complexes from spinach and their relevance to the organisation of photosystem II in vivo. *Eur J Biochem.* **243**, 422–429 (1997).
4. R. J. Porra, W. A. Thompson, P. E. Kriedemann, Determination of accurate extinction coefficients and simultaneous equations for assaying chlorophylls a and b extracted with four different solvents: verification of the concentration of chlorophyll standards by atomic absorption spectroscopy. *Biochim Biophys Acta.* **975**, 384–394 (1989).
5. C. Eijkelhoff, J. P. Dekker, Determination of the pigment stoichiometry of the photochemical reaction center of Photosystem II. *Biochim Biophys Acta.* **1231**, 21–28 (1995).
6. Y. Li, N. Scales, R. E. Blankenship, R. D. Willows, M. Chen, Extinction coefficient for red-shifted chlorophylls: Chlorophyll d and chlorophyll f. *Biochim Biophys Acta.* **1817**, 1292–1298 (2012).
7. Y. Umena, K. Kawakami, J.-R. Shen, N. Kamiya, Crystal structure of oxygen-evolving photosystem II at a resolution of 1.9 Å. *Nature.* **473**, 55–60 (2011).
8. P. Jordan *et al.*, Three-dimensional structure of cyanobacterial photosystem I at 2.5 Å resolution. *Nature.* **411**, 909–917 (2001).
9. J.-M. Ducruet, Chlorophyll thermoluminescence of leaf discs: simple instruments and progress in signal interpretation open the way to new ecophysiological indicators. *J Exp Bot.* **54**, 2419–2430 (2003).
10. N. Cox *et al.*, Identification of the Q Y Excitation of the Primary Electron Acceptor of Photosystem II: CD Determination of Its Coupling Environment. *J Phys Chem B.* **113**, 12364–12374 (2009).
11. P. Joliot, G. N. Johnson, Regulation of cyclic and linear electron flow in higher plants. *Proc Natl Acad Sci USA.* **108**, 13317–13322 (2011).
12. P. Joliot, J. Alric, Inhibition of CO₂ fixation by iodoacetamide stimulates cyclic electron flow and non-photochemical quenching upon far-red illumination. *Photosynth Res.* **115**, 55–63 (2013).
13. E. Krausz, Selective and differential optical spectroscopies in photosynthesis. *Photosynth Res.* **116**, 411–426 (2013).
14. R. C. Jennings, G. Zucchelli, E. Engelmann, F. M. Garlaschi, The long-wavelength chlorophyll states of plant LHCI at room temperature: a comparison with PSI-LHCI. *Biophys J.* **87**, 488–97 (2004).
15. P. Joliot, D. Beal, B. Frilley, Une nouvelle méthode spectrophotométrique destinée à l'étude des réactions photosynthétiques. *J Chim Phys.* **77**, 209–216 (1980).
16. S. Santabarbara, K. E. Redding, F. Rappaport, Temperature Dependence of the Reduction of P 700 + by Tightly Bound Plastocyanin in Vivo. *Biochemistry.* **48**, 10457–10466 (2009).
17. D. Béal, F. Rappaport, P. Joliot, A new high-sensitivity 10-ns time-resolution

- spectrophotometric technique adapted to in vivo analysis of the photosynthetic apparatus. *Rev Sci Instrum.* **70**, 202–207 (1999).
18. I. H. M. van Stokkum, D. S. Larsen, R. van Grondelle, Global and target analysis of time-resolved spectra. *Biochim Biophys Acta.* **1657**, 82–104 (2004).
 19. A. R. Holzwarth, in *Biophysical Techniques in Photosynthesis* (1996), pp. 75–92.
 20. J. M. Beechem, E. Gratton, M. Ameloot, J. R. Knutson, L. Brand, in *Topics in Fluorescence Spectroscopy* (1991), pp. 241–305.
 21. J. L. Hughes, P. Smith, R. Pace, E. Krausz, Charge separation in photosystem II core complexes induced by 690–730 nm excitation at 1.7 K. *Biochim Biophys Acta.* **1757**, 841–851 (2006).
 22. E. Belgio, A. P. Casazza, G. Zucchelli, F. M. Garlaschi, R. C. Jennings, Band Shape Heterogeneity of the Low-Energy Chlorophylls of CP29: Absence of Mixed Binding Sites and Excitonic Interactions. *Biochemistry.* **49**, 882–892 (2010).
 23. F. Gan *et al.*, Extensive remodeling of a cyanobacterial photosynthetic apparatus in far-red light. *Science.* **345**, 1312–1317 (2014).
 24. Y. Umena, K. Kawakami, J. R. Shen, N. Kamiya, Crystal structure of oxygen-evolving photosystem II at a resolution of 1.9 Å. *Nature.* **473**, 55–60 (2011).
 25. M. Goujon *et al.*, A new bioinformatics analysis tools framework at EMBL-EBI. *Nucl Acids Res.* **38**, W695–W699 (2010).
 26. M. Biasini *et al.*, SWISS-MODEL: Modelling protein tertiary and quaternary structure using evolutionary information. *Nucl Acids Res.* **42**, W252–W258 (2014).
 27. H. Ago *et al.*, Novel features of eukaryotic photosystem II revealed by its crystal structure analysis from a red alga. *J Biol Chem.* **291**, 5676–5687 (2016).
 28. Y. Mazar, D. Nataf, H. Toporik, N. Nelson, Crystal structures of virus-like photosystem I complexes from the mesophilic cyanobacterium *Synechocystis* PCC 6803. *Elife.* **3**, e01496 (2014).
 29. A. R. Holzwarth, J. Wendler, W. Haehnel, Time-resolved picosecond fluorescence spectra of the antenna chlorophylls in *Chlorella vulgaris*. Resolution of photosystem I fluorescence. *Biochim Biophys Acta.* **807**, 155–167 (1985).
 30. B. Gobets, R. van Grondelle, Energy transfer and trapping in photosystem I. *Biochim Biophys Acta.* **1507**, 80–99 (2001).
 31. C. W. Mullineaux, E. Bittersmann, J. F. Allen, A. R. Holzwarth, Picosecond time-resolved fluorescence emission spectra indicate decreased energy transfer from the phycobilisome to Photosystem II in light-state 2 in the cyanobacterium *Synechococcus* 6301. *Biochim Biophys Acta.* **1015**, 231–242 (1990).
 32. C. W. Mullineaux, A. R. Holzwarth, Kinetics of excitation energy transfer in the cyanobacterial phycobilisome-Photosystem II complex. *Biochim Biophys Acta.* **1098**, 68–78 (1991).
 33. E. Bittersmann, W. F. J. Vermaas, Fluorescence lifetime studies of cyanobacterial photosystem II mutants. *Biochim Biophys Acta.* **1098**, 105–116 (1991).
 34. M. Sugiura *et al.*, Energetics in photosystem II from *Thermosynechococcus elongatus* with a D1 protein encoded by either the *psbA1* or *psbA3* gene. *Biochim Biophys Acta.* **1797**, 1491–1499 (2010).
 35. H. J. van Gorkom, Identification of the reduced primary electron acceptor of Photosystem II as a bound semiquinone anion. *Biochim Biophys Acta.* **347**, 439–442 (1974).

36. M. Sugiura *et al.*, Modification of the pheophytin redox potential in *Thermosynechococcus elongatus* Photosystem II with PsbA3 as D1. *Biochim Biophys Acta*. **1837**, 139–148 (2014).
37. M. Chen, Chlorophyll Modifications and Their Spectral Extension in Oxygenic Photosynthesis. *Annu Rev Biochem*. **83**, 317–340 (2014).
38. M. Chen, Z.-L. Cai, Theoretical study on the thermodynamic properties of chlorophyll d -peptides coordinating ligand. *Biochim Biophys Acta*. **1767**, 603–609 (2007).
39. E. Schlodder *et al.*, Both chlorophylls a and d are essential for the photochemistry in photosystem II of the cyanobacteria, *Acaryochloris marina*. *Biochim Biophys Acta*. **1767**, 589–595 (2007).
40. T. Renger, E. Schlodder, The Primary Electron Donor of Photosystem II of the Cyanobacterium *Acaryochloris marina* Is a Chlorophyll d and the Water Oxidation Is Driven by a Chlorophyll a/Chlorophyll d Heterodimer. *J Phys Chem B*. **112**, 7351–7354 (2008).
41. S. P. Mielke, N. Y. Kiang, R. E. Blankenship, D. Mauzerall, Photosystem trap energies and spectrally-dependent energy-storage efficiencies in the Chl d-utilizing cyanobacterium, *Acaryochloris marina*. *Biochim Biophys Acta*. **1827**, 255–265 (2013).
42. E. L.-W. Majumder *et al.*, Subcellular pigment distribution is altered under far-red light acclimation in cyanobacteria that contain chlorophyll f. *Photosynth Res* (2017), doi:10.1007/s11120-017-0428-1.
43. M.-Y. Ho, F. Gan, G. Shen, D. A. Bryant, Far-red light photoacclimation (FaRLiP) in *Synechococcus* sp. PCC 7335. II. Characterization of phycobiliproteins produced during acclimation to far-red light. *Photosynth Res*. **131**, 187–202 (2017).
44. Y. Li *et al.*, Characterization of red-shifted phycobilisomes isolated from the chlorophyll f-containing cyanobacterium *Halomicronema hongdechloris*. *BBA - Bioenerg*. **1857**, 107–114 (2016).
45. J. R. Reimers *et al.*, Challenges facing an understanding of the nature of low-energy excited states in photosynthesis. *Biochim Biophys Acta*. **1857**, 1627–1640 (2016).
46. M. Schenderlein, M. Çetin, J. Barber, A. Telfer, E. Schlodder, Spectroscopic studies of the chlorophyll d containing photosystem I from the cyanobacterium, *Acaryochloris marina*. *Biochim Biophys Acta*. **1777**, 1400–1408 (2008).
47. S. I. Allakhverdiev *et al.*, Redox potential of pheophytin a in photosystem II of two cyanobacteria having the different special pair chlorophylls. *Proc Natl Acad Sci USA*. **107**, 3924–3929 (2010).
48. Y. Kato, M. Sugiura, A. Oda, T. Watanabe, Spectroelectrochemical determination of the redox potential of pheophytin a, the primary electron acceptor in photosystem II. *Proc Natl Acad Sci USA*. **106**, 17365–17370 (2009).
49. J. H. Golbeck, Ed., *Photosystem I. The Light-driven Plastocyanin: Ferredoxin Oxidoreductase* (Springer Netherlands, 2006).